Available online at www.sciencedirect.com

ScienceDirect

Geochimica et Cosmochimica Acta 157 (2015) 164–181

Geochimica et Cosmochimica Acta

www.elsevier.com/locate/gca

Experimental calibration of Mg isotope fractionation between dolomite and aqueous solution and its geological implications

Weiqiang Li [a,b,c,*], Brian L. Beard [a,b], Chengxiang Li [c], Huifang Xu [a,b], Clark M. Johnson [a,b]

[a] University of Wisconsin-Madison, Department of Geoscience, 1215 West Dayton Street, Madison, WI 53706, United States
[b] NASA Astrobiology Institute, United States
[c] State Key Laboratory for Mineral Deposits Research, School of Earth Sciences and Engineering, Nanjing University, Nanjing 210093, PR China

Received 24 September 2014; accepted in revised form 19 February 2015; Available online 7 March 2015

Abstract

Hydrothermal experiments at 220, 160, and 130 °C were performed to calibrate the Mg isotope fractionation factor between dolomite and aqueous Mg. Hydrothermal experiments included synthesis of dolomite using different starting materials, as well as exchange experiments that used poorly-ordered proto-dolomite. The morphology of synthesized dolomite was dependent on starting mineralogy, suggesting that dolomite was synthesized by different pathways. Hydrothermally synthesized dolomite was initially fine-grained disordered or poorly-ordered dolomite that, with time, recrystallized to coarser-grained ordered dolomite. Isotopic exchange was monitored using $^{87}Sr/^{86}Sr$ ratios and ^{25}Mg tracers, and these indicated near-complete isotope exchange between dolomite and aqueous solutions at the end of most hydrothermal experiments. The Mg isotope fractionation factor between dolomite and aqueous solution obtained from synthesis and exchange experiments converged with time and was independent of dolomite morphology, suggesting attainment of isotopic equilibrium. Combining results from synthesis and exchange experiments, the temperature dependent Mg isotope fractionation factor for ordered dolomite is:

$$\Delta^{26}Mg_{dolo-aq} = -0.1554(\pm 0.0096) \times 10^6/T^2$$

where T is in Kelvin. In contrast, poorly-ordered dolomite has a $\Delta^{26}Mg_{dolo\text{-}aq}$ fractionation factor that is up to 0.25‰ lower than that of ordered dolomite, and this is attributed to longer Mg–O bonds in imperfectly ordered dolomite. The experimentally calibrated $\Delta^{26}Mg_{dolo\text{-}aq}$ fractionation factors lie between those calculated by Schauble (2011) and Rustad et al. (2010). The $\Delta^{26}Mg_{dolo\text{-}aq}$ fractionation factor extrapolated to lower temperatures using the $\Delta^{26}Mg$-T function of this study matches the $\Delta^{26}Mg_{dolo\text{-}aq}$ fractionation factor obtained by modeling of Mg isotope compositions of ODP drill core samples. This study shows that significant Mg isotope fractionation occurs during dolomite precipitation. These results collectively demonstrate that Mg isotopes in dolomite are a useful tool for studying Mg global cycling and dolomitization.

1. INTRODUCTION

Dolomite [$MgCa(CO_3)_2$] is an important Mg-bearing carbonate mineral, and dolomite-bearing lithologies comprise a major component of the ancient carbonate record.

* Corresponding author at: School of Earth Sciences and Engineering, Nanjing University, Nanjing 210093, PR China. Tel.: +86 13270805920.
E-mail addresses: liweiqiang@nju.edu.cn, liweiq@gmail.com (W. Li).

http://dx.doi.org/10.1016/j.gca.2015.02.024
0016-7037/

Up to 50% of the world's carbonate reservoirs for oil and gas occur in dolomite (Zenger et al., 1980). Moreover, dolomite hosts most Mississippi Valley-type (MVT) Zn–Pb deposits, as well as many skarn-type ore deposits (Warren, 2000). The relative abundance of dolomite in sedimentary rocks has varied throughout geological time, comprising the major proportion of carbonate rocks deposited in the Ordovician to Early Carboniferous and Triassic to Mid Cretaceous, but lesser proportions at other times in the Phanerozoic (Given and Wilkinson, 1987). Throughout the Phanerozoic, the cyclical change in dolomitization intensity has been broadly correlated with long-term rhythmic changes in sea level (e.g., Vail et al., 1977), mineralogy of primary seawater calcium carbonates (e.g., Sandberg, 1983; Stanley and Hardie, 1998), seawater chemistry (e.g., Lowenstein et al., 2001), and atmospheric pCO_2 levels (e.g., Fischer, 1984), suggesting that sedimentary dolomite may contain clues to understanding secular changes in Earth's climatic and environmental parameters (Burns et al., 2000).

Stable Mg isotopes are an emerging geochemical tool, and it has great potential for studying dolomite-related problems. For example, controversy remains on the cause of secular changes in seawater Mg/Ca ratios in the Phanerozoic, where some workers propose that it was caused by variations in the intensity of dolomite formation (Wilkinson and Algeo, 1989; Holland, 2005), but others argue that it was mainly controlled by the intensity of mid-ocean ridge hydrothermal activity (Spencer and Hardie, 1990; Hardie, 1996). If there is a contrast in Mg isotope fractionation between the processes of dolomitization and water–rock reaction during mid-ocean ridge hydrothermal activity, then stable Mg isotopes may be used to test competing hypotheses for secular changes in seawater Mg/Ca ratios in the Phanerozoic.

The confidence with which Mg isotopes may be currently applied to dolomite-related geological problems is limited by the lack of knowledge of Mg isotope fractionation during dolomite precipitation. Equilibrium Mg isotope fractionation factors between dolomite and aqueous solution have been predicted using *ab initio* approaches, but the results are inconsistent. Schauble (2011) predicted that dolomite is enriched in light Mg isotopes relative to aqueous solution, whereas Rustad et al. (2010) predicted an opposite direction for Mg isotope fractionation. At 20 °C, the inconsistency in calculated fractionation factors for dolomite between the two studies is over 5‰ in $^{26}Mg/^{24}Mg$ ratio, which is comparable to the entire range of natural Mg isotope variation that has been reported (Saenger and Wang, 2014; and references therein). Magnesium isotope fractionation factors between dolomite and fluid (defined as $\Delta^{26}Mg_{min\text{-}aq}$ for $^{26}Mg/^{24}Mg$ ratios) have been also estimated from determination of natural mineral/rock-solution pairs, but such data are not systematic, and do not point to a consistent fractionation factor (e.g., −2.0‰ in Fantle and Higgins, 2014; −0.7‰ to +0.1‰ in Geske et al., 2015b; −2.7‰ to −2.0‰ in Higgins and Schrag, 2010).

Experimental calibration of Mg isotope fractionation factors has proven challenging. Abiotic synthesis of dolomite at ambient temperatures is notoriously difficult (e.g., Land, 1998), and this, together with the scarce occurrence of dolomite precipitates in modern and Holocene sedimentary rocks, have been commonly referred to as the "dolomite problem" (e.g., Zenger et al., 1980; Burns et al., 2000; Warren, 2000). It is generally agreed that the "dolomite problem" is a kinetic issue, where high energy barriers inhibit dehydration of $Mg(H_2O)_6^{2+}$ at low temperatures (e.g., Land, 1998). Although $Mg(H_2O)_6^{2+}$ dehydration and dolomite precipitation can be catalyzed by sulfate-reducing microbes (e.g., Vasconcelos et al., 1995) and the presence of polysaccharide or dissolved sulfide in solution (Zhang et al., 2012a,b), kinetic effects for Mg isotope fractionation produced under various experimental conditions during of Mg-calcite precipitation (Immenhauser et al., 2010; Mavromatis et al., 2013) raises the possibility that pathway-dependent kinetic isotope effects may affect experimentally measured dolomite-fluid fractionation factors during dolomite synthesis.

Because it is difficult to assess the contribution of kinetic effects for Mg isotopes during low-temperature precipitation of dolomite, we did not attempt experiments at room temperatures. Instead, we calibrated Mg isotope fractionation factors for dolomite at moderate hydrothermal conditions, where inorganic synthesis of dolomite has been widely reported (e.g., Graf and Goldsmith, 1956; Rosenberg and Holland, 1964; Katz and Matthews, 1977; Sibley et al., 1994; Kaczmarek and Sibley, 2011). In addition to synthesis experiments, we conducted isotopic exchange experiments through recrystallization of disordered dolomite at hydrothermal conditions, and constrained the degree of isotopic exchange between solid and aqueous phases using a ^{25}Mg tracer, as well as through use of contrasting $^{87}Sr/^{86}Sr$ ratios in the starting materials. Combining the synthesis and exchange experiments, we converge on the likely equilibrium Mg isotope fractionation factors for dolomite formation at 130, 160, and 220 °C, allowing us to establish the temperature dependence of Mg isotope fractionation for dolomite, which is an important first step towards understanding Mg isotope behavior during dolomitization over greater temperature ranges.

2. EXPERIMENTAL METHODS

2.1. Hydrothermal experiments

To evaluate if there is pathway dependence for Mg isotope fractionation during dolomite hydrothermal synthesis, a multi-direction approach was used. This included synthesis of dolomite from aragonite, calcite, and nesquehonite ($MgCO_3 * 3H_2O$). Aragonite powder was prepared from pulverizing a gem-quality aragonite crystal (origin: Sefrou, Morocco) in a ball mill. Analytical-grade calcite powder was purchased from Sigma–Aldrich®. Nesquehonite was prepared in-house by mixing a saturated $MgCl_2$ solution and 1 M Na_2CO_3 solution in an ultrasonic bath for 30 min, followed by washing and centrifugation three times with de-ionized water. Calcium carbonates (aragonite and calcite) were reacted with gravimetrically prepared "stock solution A", which contained 1.0 M

$CaCl_2$, 1.0 M $MgCl_2$, and 123 ppm Sr. Nesquehonite was reacted with "stock solution B", which contained 1.5 M $CaCl_2$ and 0.5 M $MgCl_2$ that was enriched in ^{25}Mg.

For dolomite exchange experiments, disordered dolomite was synthesized with Mg that was spiked with a ^{25}Mg tracer, followed by recrystallization in "stock solution A" at hydrothermal conditions. The "spiked disordered dolomite" was prepared by reacting 1 g of aragonite powder with 15 mL of "stock solution C" in a sealed Teflon-lined Parr® Bomb in a conventional oven at 220 °C for 2.5 h. "Stock solution C" was prepared by mixing 20 mL "stock solution A" with 3.05×10^{-5} mol of ^{25}Mg spike (^{24}Mg: 0.80%, ^{25}Mg: 98.88%, ^{26}Mg: 0.32%; purchased from Oak Ridge National Lab). The ^{25}Mg tracer was used to monitor the degree of Mg isotope exchange between solid and aqueous phases during mineral recrystallization, as reported in previous studies (Li et al., 2011, 2014).

Hydrothermal synthesis or exchange experiments were carried out in a closed reaction vessel made of a 4 cm long, 4.6 mm inner diameter gold or silver tube using a cold-seal technique (Komareneni et al., 1979), or a tightly capped 3 mL PFA beaker. A reaction vessel typically contained ca. 0.35 ml of aqueous solution and 5–10 mg of mineral powder. Details of experimental conditions for each set of hydrothermal experiments are tabulated in Table 1. The reaction vessel was placed in a Parr® bomb, and about 10 ml water was added to the bomb for vapor pressure balance at elevated temperature, then the bomb was sealed and placed in a gravity convection oven with temperature preset at 130, 160, or 220 °C. Repeat measurements of oven temperature indicated that the temperature was stable within ±1 °C at 130 °C, ±2 °C at 160 °C and ±4 °C at 220 °C. In general, each set of synthesis or exchange experiments used multiple (up to 5) reaction vessels/bombs that contained identically prepared mixtures of solution and mineral, and the reaction vessels/bombs were sampled in a time series in an exponential fashion. Opening of oven door and sampling of hydrothermal bombs took less than 30 s, and produced a <10 °C transient drop in air temperature in the oven, which was typically recovered within 5 min. Considering the thick wall, large mass, and heat capacity of the bombs and contained fluid, such transient temperature fluctuations were not expected to affect the reaction temperature inside the hydrothermal bombs more significantly than the overall temperature variations of the oven noted above.

Reaction vessels were sampled and weighed after quenching the hydrothermal bombs in air to room temperature within two hours. Typically, the weight change of reaction vessels before and after an experiment was within ±10 mg for sealed gold or silver tubes, or within ±50 mg for 3 mL PFA beakers. Reaction vessels with obvious leakages (e.g., >100 mg weight change) were discarded. The solid and fluid phases from the experiments were separated using a centrifuge tube with a 0.22 μm filter bottom. Upon separation, the solid phase was further washed with de-ionized water and centrifuged three times to remove interstitial fluids.

2.2. Mineral characterization

Mineral morphology was characterized using a Hitachi S-3400N scanning electron microscope using backscattered

Table 1
Summary of experiments.

Experiment ID	Temp. (°C)	Reaction vessel	Starting material	Experimental duration	Mineralogy of product (by XRD)
Synthesis experiments					
Arag220	220 ± 4	Gold capsule	7.0 mg of aragonite + 0.3 mL of "stock solution A"*	4, 8, 12, 81, and 315 h	Pure dolomite for all experiments
Arag220s	220 ± 4	Teflon liner of Parr® bomb	1 gram of aragonite + 15 mL of "stock solution A" that is spiked with ^{25}Mg	2.5 h	Pure disordered dolomite
Arag160	160 ± 2	Silver capsule	7.0 mg of aragonite + 0.3 mL of "stock solution A"*	1, 6, 13, 28, and 52 days	Pure dolomite for all experiments, except the sample after 1 day
Arag130	130 ± 1	Teflon beaker	18.7 mg of aragonite + 0.8 mL of "stock solution A"*	10 days	Aragonite (67.7%), dolomite (30.3%), Mg-calcite (2.0%),
Calc220	220 ± 4	Silver capsule	7 mg of calcite + 0.3 mL of "stock solution A"	81 and 315 h	Pure dolomite for both experiments
Nesq160	160 ± 2	Teflon beaker	19.4 mg of nesquehonite + 2 mL "stock solution B"**	6 days	Pure dolomite
Nesq130	130 ± 1	Teflon beaker	34.5 mg nesquehonite + 2 mL "stock solution B"**	10 days	Dolomite (76.5%), Mg-calcite (23.5%)
Recrystallization experiments					
Dex220	220 ± 4	Gold capsule	1.5 mg of ^{25}Mg-spiked disordered dolomite + 0.3 mL of "stock solution A"*	2, 5, and 12 days	Pure dolomite for all experiments
Dex160	160 ± 2	Gold capsule	1.5 mg of ^{25}Mg-spiked disordered dolomite + 0.3 mL of "stock solution A"*	5, 12, and 22 days	Pure dolomite for all experiments
Dex130	130 ± 1	Teflon beaker	1.5 mg of ^{25}Mg-spiked disordered dolomite + 0.3 mL of "stock solution A"*	1, 3, 9, and 20 days	Mg-calcite (58.3–0%), dolomite (41.7–100%)

* "Stock solution A" contains 1.0 M $CaCl_2$, 1.0 M $MgCl_2$, and 124 ppm Sr.
** "Stock solution B" contains 1.5 M $CaCl_2$, and 0.5 M ^{25}Mg-enriched $MgCl_2$.

electron (BSE) mode. Spot analyses using Energy-Dispersive X-ray Spectroscopy (EDS) were performed using an accelerating voltage of 15 kV, a working distance of 10 mm, and Thermo Scientific NORAN System SIX software. XRD analysis was performed on a Rigaku Rapid II X-ray diffraction system, using a Mo target X-ray source (Mo $K_\alpha = 0.71073$ Å) and a 0.3 mm diameter beam. Powder material (typically less than 1 mg) was loaded onto a glass fiber for transmission-mode XRD analysis. Diffraction data were collected on a 2-D image-plate detector, and were converted to produce conventional 2θ vs. intensity patterns using Rigaku 2DP software. Interpretation and Rietveld refinement of the XRD patterns were made using Jade 9.5 software. For solid samples of mineral mixtures, the proportion of each mineral was calculated by fitting the XRD pattern using the Rietveld method, and the uncertainty of the calculation is estimated at <5 wt.%.

2.3. Isotope analysis

Prior to isotopic analysis, aliquots of the solid and aqueous samples were treated with concentrated HNO_3 and dried repeatedly, to transform cations to nitrate form for ion-exchange chromatography. Magnesium was purified using an established two-stage column procedure, first on a column that contained 0.3 mL of Biorad AG50W × 8 cation exchange resin, then on a column that contained 0.3 mL of Eichrom DGA resin (for details, see Li et al., 2012, 2014). Recovery of Mg was >98%, and total procedural blanks for the ion-exchange procedure were negligible (Li et al., 2012, 2014).

Magnesium isotope analyses were made using a Nu Plasma II MC-ICP-MS, a double-focusing mass spectrometer. The instrument was operated in low-mass-resolution mode, typically using a ~80 μL/min self-aspirating nebulizer tip and a cyclonic spray chamber cooled to 7 °C. Magnesium isotope ratios were measured using a standard-sample-standard bracketing method and a 1 ppm in-house standard solution. The concentration of samples typically matched the bracketing standard to better than ±5%. A 60 s on-peak acid blank was measured before each analysis. Each Mg isotope ratio measurement consisted of sixty 5-s integrations, and the typical internal precision (2 standard error or 2SE) was better than ±0.04‰ for $^{26}Mg/^{24}Mg$ and ±0.02‰ for $^{25}Mg/^{24}Mg$. The long-term external reproducibility (2 standard deviation or 2SD) of Mg isotope analysis is better than ±0.10‰ in $^{26}Mg/^{24}Mg$ and ±0.05‰ in $^{25}Mg/^{24}Mg$ over six months, based on repeat analysis of multiple Mg isotope standard solutions against in-house stock solutions (Appendix 1). Further details of mass spectrometry procedures for Mg isotope analysis can be found in Li et al. (2014).

Magnesium isotope compositions are reported using the standard per mil (‰) notation of $\delta^{26}Mg$ for the $^{26}Mg/^{24}Mg$ isotope ratios relative to the DSM3 Mg isotope standard (Galy et al., 2003), where

$$\delta^{26}Mg = [(^{26}Mg/^{24}Mg_{sample})/(^{26}Mg/^{24}Mg_{DSM3}) - 1] \times 1000 \quad (1)$$

$\delta^{25}Mg$ values for the $^{25}Mg/^{24}Mg$ ratios are reported using a similar formulation. Fractionation in Mg isotopes between two phases A and B is expressed as:

$$\Delta^{26}Mg_{A-B} = \delta^{26}Mg_A - \delta^{26}Mg_B \approx 10^3 \ln\alpha^{26/24}_{A-B} \quad (2)$$

The error in Mg isotope fractionation factors is calculated by the error propagation function:

$$Err\Delta Mg_{A-B} = \left[(Err\delta Mg_A)^2 + (Err\delta Mg_B)^2\right]^{1/2} \quad (3)$$

where $Err\Delta Mg_{A-B}$ is the error of Mg isotope fractionation factor, and $Err\delta Mg_A$ and $Err\delta Mg_B$ are the analytical errors for phase A and B, respectively.

The accuracy of the total analytical method was monitored by analysis of test solutions that were processed along with samples using the ion-exchange procedure noted above. The test solutions were made of equal-molar amounts of the in-house Mg standard HPS909104 and $CaCl_2$ to mimic the samples from the dolomite experiments. The measured $\delta^{26}Mg$ values for the six test solutions match that of HPS909104 within ±0.07‰ (2SD, Table 2), within the external reproducibility, and consistent with the accuracy of Mg isotope measurements for various matrices (Mg-sulfate, low Mg calcite, seawater, brucite, Mg-EDTA, etc.) in previous studies from the laboratory (Li et al., 2011, 2012, 2014).

Strontium isotope analysis of solid and fluid phases was performed on a VG *Sector 54* thermal ionization mass spectrometer, following Sr purification using Eichrom Sr-Spec resin and HNO_3. Details of the analytical methods are reported previously (Beard et al., 2013). Typical internal error for $^{87}Sr/^{86}Sr$ ratio measurements was better than 10 ppm. Repeat analyses of NIST SRM-987 during the analytical session gave an average $^{87}Sr/^{86}Sr$ ratio of 0.71027 ± 0.00002 (2SD, $n = 11$). Strontium concentrations of starting materials for synthesis experiments ("stock solution A", aragonite, and calcite) were measured by isotope-dilution mass spectrometry using a mixed ^{87}Rb–^{84}Sr spike.

3. RESULTS

3.1. Synthesis experiments

3.1.1. Mineralogy

The mineralogy of the products for the synthesis experiments is summarized in Table 1. Briefly, at the same temperature, it takes less time to synthesize dolomite using aragonite (2.5 h at 220 °C) than using calcite (81 h at 220 °C) (Table 1). Given the same starting solution and mineral, it takes less time to synthesize dolomite at higher temperatures, where, for example, aragonite was completely transformed to dolomite after 2.5 h of reaction at 220 °C and 6 days of reaction at 160 °C (Table 1, Appendix 2). For synthesis experiments at 130 °C, reaction was incomplete and contained mixtures of dolomite and other minerals (Table 1, Appendix 2).

There are distinct differences in morphology of the synthesized dolomite between experiments with different starting materials. Synthesis experiments using aragonite as the starting material typically produced homogenous,

Table 2
Isotopic and mineralogical parameters of samples in synthesis experiments.

EXP. or Sample No.	Time (days)	Solution					Solid					Fractionation (solid-aq)				Dolomite XRD			Solution		solid	
		$\delta^{26/24}$Mg	2SD	$\delta^{25/24}$Mg	2SD	$n(N)$*	$\delta^{26/24}$Mg	2SD	$\delta^{25/24}$Mg	2SD	n(N)*	$\Delta^{26/24}$Mg	2SD	$\Delta^{25/24}$Mg	2SD	D(104) (Å)	FWHM (104)	I(105)/ I(110)	^{87}Sr/^{86}Sr	2SE	^{87}Sr/^{86}Sr	2SE
test solution**		−0.68	0.07	−0.36	0.03	16(6)																
Starting material																						
"stock solution A"		−1.54	0.09	−0.79	0.05	15(6)													0.70984	0.0008		
"stock solution B"		−1.25	0.06	12.60	0.01	2(1)																
"stock solution C"		−1.63	0.07	12.40	0.03	4(1)																
Aragonite																					0.70944	0.0007
Calcite																					0.70798	0.0007
Synthesis exp																						
Arag220s	0.08	−1.25	0.06	12.60	0.01	2(1)	−2.00	0.04	12.14	0.03	7(2)	−0.75	0.08	−0.46	0.04	2.914	0.339	0.05				
Arag220	0.17	−1.36	0.12	−0.71	0.06	4(1)	−2.27	0.08	−1.17	0.04	4(1)	−0.91	0.15	−0.46	0.07	2.905	0.255	0.11	0.70977	0.0008		
	0.33	−1.54	0.13	−0.79	0.07	4(1)	−2.28	0.07	−1.18	0.04	2(1)	−0.74	0.15	−0.39	0.08	2.893	0.175	0.25	0.70978	0.0008		
	0.50	−1.37	0.05	−0.72	0.03	3(1)	−2.27	0.04	−1.17	0.04	3(1)	−0.90	0.06	−0.45	0.05	2.891	0.180	0.44	0.70977	0.0007		
	3.38	−1.58	0.04	−0.81	0.02	3(1)	−2.24	0.03	−1.15	0.02	3(1)	−0.66	0.05	−0.34	0.03	2.891	0.167	0.36	0.70979	0.0007		
	13.13	−1.55	0.08	−0.79	0.06	3(1)	−2.27	0.06	−1.18	0.04	3(1)	−0.72	0.11	−0.39	0.07	2.890	0.173	0.35	0.70977	0.0008		
Arag160	1	−1.55	0.13	−0.80	0.06	3(1)	−2.66	0.03	−1.37	0.04	3(1)	−1.11	0.13	−0.57	0.07	2.925	0.285	0.01	0.70981	0.0010	0.70945	0.0007
	6	−1.54	0.01	−0.81	0.01	2(1)	−2.49	0.12	−1.28	0.04	3(1)	−0.95	0.12	−0.48	0.04	2.895	0.184	0.39	0.70976	0.0007	0.70978	0.0007
	13	−1.52	0.02	−0.77	0.00	2(1)	−2.52	0.06	−1.30	0.01	3(1)	−1.00	0.06	−0.52	0.01	2.890	0.181	0.32	0.70975	0.0007	0.70977	0.0007
	28	−1.51	0.03	−0.79	0.03	2(1)	−2.49	0.15	−1.28	0.07	3(1)	−0.97	0.15	−0.50	0.08	2.894	0.179	0.37	0.70975	0.0008	0.70975	0.0007
	52	−1.55	0.08	−0.80	0.04	5(1)	−2.44	0.07	−1.26	0.04	4(1)	−0.89	0.11	−0.46	0.06	2.892	0.196	0.43				
Arag130	10	−1.51	0.03	−0.79	0.02	3(1)	−2.41	0.04	−1.27	0.04	3(1)	−0.90	0.05	−0.48	0.04	2.930	0.314	0.00				
	70															2.900	0.197	0.29				
Calc220	3.38	−1.42	0.05	−0.73	0.02	3(1)	−2.26	0.05	−1.17	0.03	4(1)	−0.84	0.07	−0.44	0.03	2.890	0.201	0.48	0.70982	0.0007	0.70982	0.0007
	13.13	−1.49	0.06	−0.77	0.03	3(1)	−2.13	0.01	−1.10	0.02	2(1)	−0.65	0.06	−0.34	0.03	2.890	0.185	0.50	0.70983	0.0007	0.70980	0.0013
Nesq160	6	−1.38	0.02	11.71	0.01	2(1)	−2.33	0.06	11.20	0.02	2(1)	−0.94	0.07	−0.51	0.02	2.900	0.246	0.33				
Nesq130	10	−1.35	0.04	11.18	0.03	2(1)	−2.46	0.07	10.55	0.04	2(1)	−1.11	0.08	−0.63	0.05	2.911	0.229	0.14				

* n denotes total number of isotope analysis, N denotes number of replicates.
** Test solution contains 2 μmol of $MgCl_2$ (HPS909104, $\delta^{26}Mg = -0.66‰$) and 2 μmol of $CaCl_2$.

fine-grained (1–5 μm in size), well dispersed, euhedral rhombohedrons of dolomite (Fig. 1, image A2, A3), despite the huge variation in grain size of the starting aragonite (a few to over 100 μm, Fig. 1, image A1). Synthesis experiments using calcite as the starting material, however, produced dolomite aggregates that apparently retained the 5–20 μm-sized rhomboheral morphology of the original calcite crystals, but with numerous sub-micron-sized cavities/pits (Fig. 1, image B2, B3). Such morphology has been reported in previous dolomite synthesis experiments using calcite, and was referred to as "Swiss cheese" texture in previous work (Katz and Matthews, 1977). Synthesis experiments using nesquehonite as the starting material produced spherical aggregates 5–30 μm in diameter of fine-grained dolomite crystals (and Mg-calcite for 130 °C experiment) (Fig. 1, image C2), and these are fundamentally different compared to the rod-like shape of the starting nesquehonite.

There are systematic changes in crystal size and XRD patterns of the synthesized dolomite in time-series synthesis experiments. In experiments that used aragonite as the starting material, where synthesized dolomite occurred as dispersed homogenous crystals, the crystal size of dolomite increased with time. For example, in experiment series

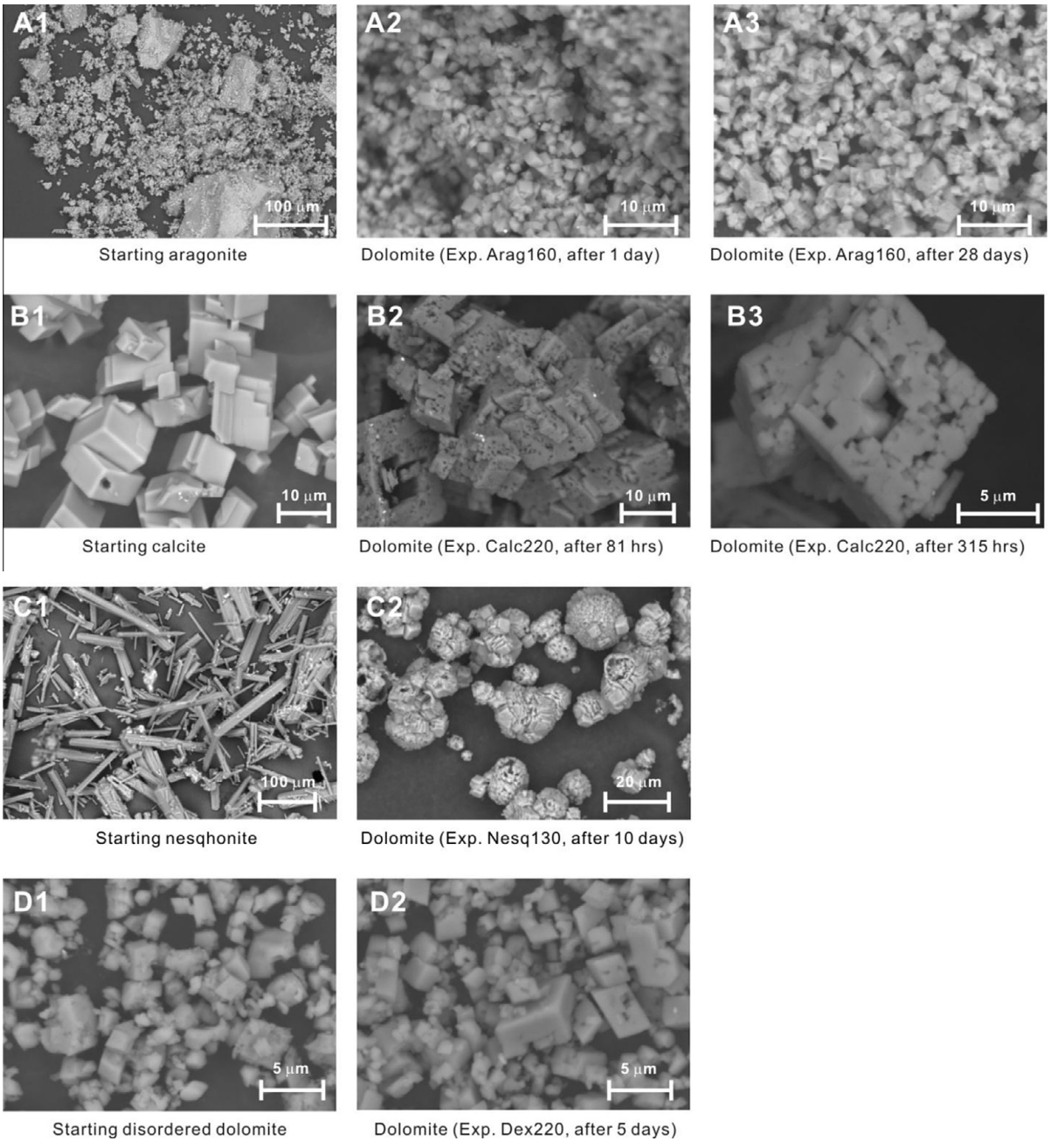

Fig. 1. SEM images of starting minerals and products of hydrothermal experiments. For details of experiments, see Table 1.

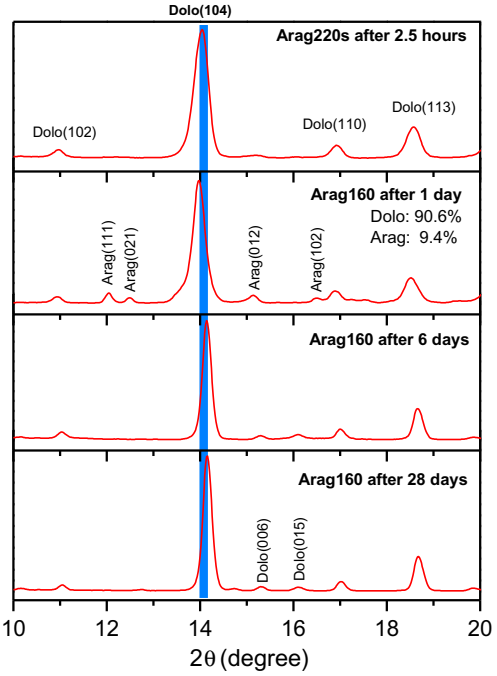

Fig. 2. XRD spectra of synthesized dolomite showing decrease of peak width and increase in the 2θ value of (104) peak for dolomite with increasing reaction time. The solid product of experiment Arag160 after 1 day contained minor aragonite (9.4 wt.%, determined by Rietveld refinement), whereas other samples were pure dolomite. Note the appearance of (015) peak with increasing reaction time, which suggests ordering of dolomite.

"Arag160" (see Table 1), the size of dolomite crystals after 1 day of synthesis at 160 °C tightly clustered around 1–2 μm (Fig. 1, image A2), but after 28 days, the size of dolomite crystals increased to 2–5 μm (Fig. 1, image A3). Consistent with SEM observations, the XRD peak width of dolomite decreased with reaction time (Fig. 2), also indicating crystal coarsening and an increase in crystallinity. A quantitative measure of the XRD peak width can be made using the full-width-half-maximum (FWHM) of the dolomite (104) peak. The FWHM of the (104) dolomite peak decreased from >0.25 at the beginning of the experiments to <0.2 at the end of the experiments (Table 2, Figs. 2 and 3). Accompanying the decrease in FWHM of the dolomite (104) peak was a decrease in the d value of the (104) peak, that decreased from ~2.93 to ~2.89 with increasing reaction time in each of the time-series synthesis experiments (Table 2, Fig. 3A). In addition, the peak intensity ratio between the (105) peak and the (110) peak (e.g., $I(105)/I(110)$), which is a measurement of the ordering of cations in the dolomite lattice (e.g., Graf and Goldsmith, 1956), increased with synthesis reaction time (Figs. 2 and 3, Table 2), from 0.010.11 to 0.35–0.50. In general, there is a positive correlation between FWHM and d value of peak (104) (Fig. 3B), and a negative correlation between $d(104)$ and $I(105)/I(110)$ (Fig. 3C).

3.1.2. Isotope results

In all synthesis experiments, solid products have lower $\delta^{26}Mg$ values than those of the aqueous solutions, regardless of experimental conditions, and staring materials (Table 2). The apparent Mg isotope fractionation factor between solid and aqueous phases of the experiments ($\Delta^{26}Mg_{min\text{-}aq}$) showed a general temperature dependence (Fig. 4). Synthesis experiments at 220 °C (exps. Arag220, Arag220s, calc220) produced $\Delta^{26}Mg_{min\text{-}aq}$ fractionations between −0.91‰ and −0.65‰, and synthesis experiments at 160 °C (exps. Arag160, Nesq160) produced $\Delta^{26}Mg_{solid\text{-}aq}$ fractionations between −1.11‰ and −0.89‰ (Table 2). In synthesis experiments at 130 °C, where non-dolomite Mg-bearing minerals were identified from the solid products (Table 1), the $\Delta^{26}Mg_{solid\text{-}aq}$ fractionations were −1.10‰ for exp. Nesq130 and −0.90‰ for exp. Arag130 (Table 2). In addition, time-series experiments of aragonite (Arag220, Arag160) showed that the measured $\Delta^{26}Mg_{solid\text{-}aq}$ fractionations increased with reaction time, as the lower $\Delta^{26}Mg_{solid\text{-}aq}$ fractionations generally occurred in the earlier sampled reaction vessels and higher $\Delta^{26}Mg_{solid\text{-}aq}$ fractionations generally occurred in the later sampled reaction vessels, although the 2SD error bars of the $\Delta^{26}Mg_{solid\text{-}aq}$ fractionations for the same time-series experiment overlap (Fig. 4).

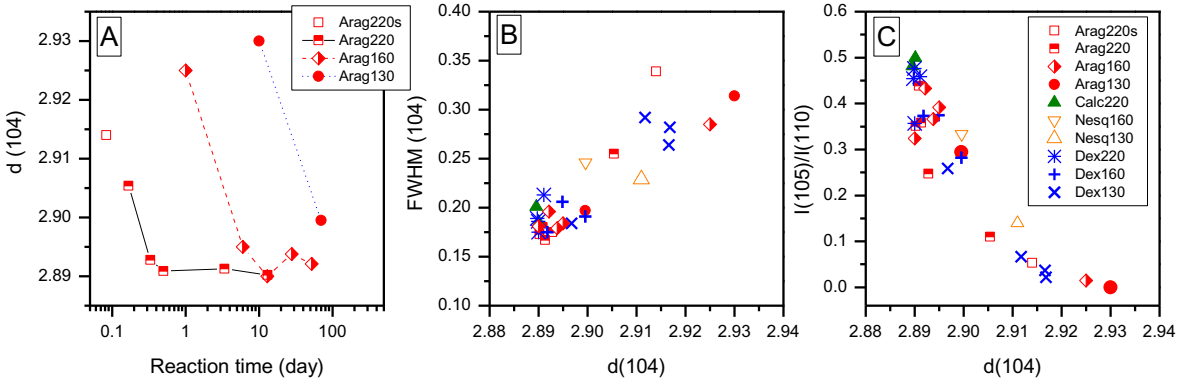

Fig. 3. XRD parameter plots for dolomite in this study. (A) dolomite $d(104)$ versus reaction time for synthesis experiments using aragonite as the starting material, (B) $d(104)$ value versus peak width of (104) peak (full-width-half-maximum, or FWHM of (104)) for dolomite, (C) $d(104)$ value versus $I(105)/I(110)$ or intensity ratio between peak (105) and peak (110).

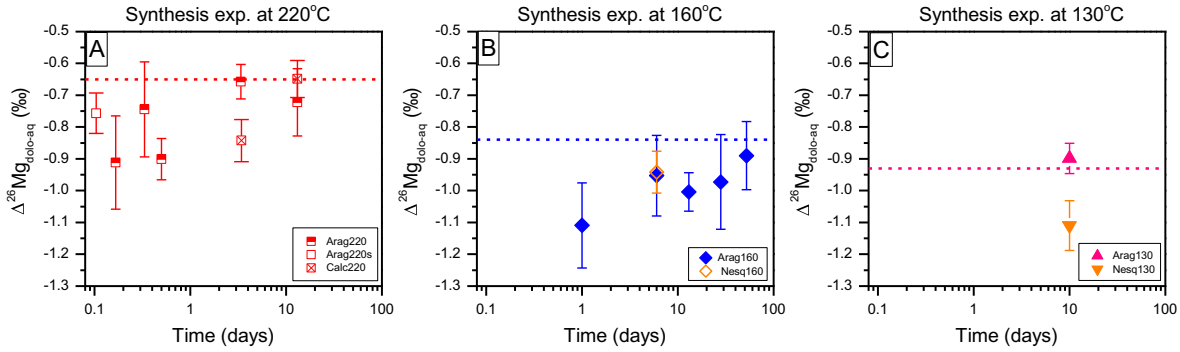

Fig. 4. Summary of measured apparent $\Delta^{26}Mg_{dolo\text{-}aq}$ fractionation factors obtained from synthesis experiments. For comparison, the estimates of equilibrium $\Delta^{26}Mg_{dolo\text{-}aq}$ fractionation factors at 220, 160, and 130 °C, based on exchange experiments, are plotted as dash lines. For details about the equilibrium fractionation factors, see Section 4.3. Error bar denotes 2 standard deviation (95% confidence level). The uncertainty of the estimated equilibrium fractionation factor is ±0.05‰ or less (see Section 4.3).

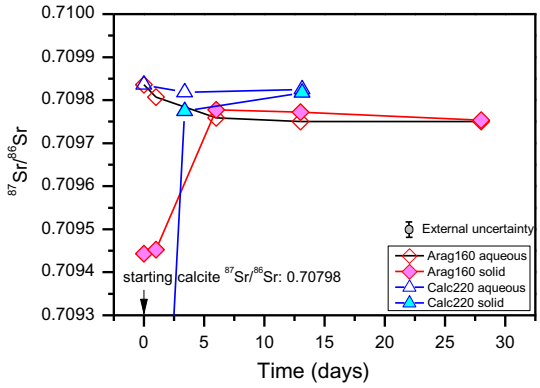

Fig. 5. Strontium isotope composition of aqueous and solid phases of selected synthesis experiments.

In synthesis experiments, we used $^{87}Sr/^{86}Sr$ ratios to monitor elemental exchange during dolomite formation. The starting aragonite and calcite contain 2223 and 89 ppm of Sr, and $^{87}Sr/^{86}Sr$ ratios of 0.70944 and 0.70799, respectively. The $^{87}Sr/^{86}Sr$ ratio of the starting minerals were significantly lower than that of the "stock solution A" ($^{87}Sr/^{86}Sr = 0.70984$, 124 ppm). In experiment series Arag160, the $^{87}Sr/^{86}Sr$ ratios of aqueous solution and solid phase converged with time, towards a value of 0.70975 (Table 2, Fig. 5). In experiment series Calc220, the $^{87}Sr/^{86}Sr$ ratios of aqueous solution and solid phase also changed, converging to 0.70982 (Table 2, Fig. 5). The final Sr isotope compositions are consistent with the respective isotope mass balance for the two experiment series ($^{87}Sr/^{86}Sr = 0.70975$ for exp. Arag160, and 0.70982 for exp. Calc220), suggesting that Sr in solid and aqueous phases was homogenized during dolomitization in the synthesis experiments.

3.2. Exchange experiments

3.2.1. Mineralogy

The starting material ("spiked proto-dolomite") for the exchange experiments was the solid product of synthesis experiment Arago220s (Table 1). XRD analysis shows that the starting "spiked proto-dolomite" had a low degree of ordering [$I(105)/I(110) = 0.05$], a high $d(104)$ value (2.914 Å), and a wide (104) peak width (FWHM = 0.339). The grain size of the starting "spiked proto-dolomite" varied between 0.5 and 4 μm. It should be noted that the grains were mostly irregular in shape and did not have a rhombohedral habit, indicating a low degree of crystallinity (Fig. 1, image D1). Exchange experiments at 220 °C significantly increased the ordering of the dolomite, as $I(105)/I(110)$ ratios increased to 0.45–0.48 after 12 days; for recrystallization experiments at 160 °C, the ordering also increased but to a lesser degree; $I(105)/I(110)$ was 0.37 after 22 days of reaction (Table 3).

Exchange experiments at 130 °C resulted in an abrupt appearance of Mg-bearing calcite in the solid phase after the first day of reaction. This was distinct from the exchange experiments at 160 and 220 °C, where dolomite remained the sole mineral over the duration of the experiments. Rietveld refinement of the XRD pattern showed that Mg-calcite consisted of 58.3 wt% of the solid, and the rest was dolomite (Fig. 6, Appendix 2). The abundance of Mg-calcite decreased with increasing experimental duration and ultimately after 20 days all the Mg-calcite was converted to dolomite (Fig. 6, Appendix 2). Despite the increase in relative abundance of dolomite, dolomite remained poorly ordered and poorly crystalline. For example, in the first 9 days of reaction at 130 °C $I(105)/I(110)$ was low (0.02–0.07), and peak width was large (FWHM of (104) peak = 0.292–0.264) (Table 3). After 20 days of reaction, when all Mg-calcite disappeared, the degree of ordering and crystallinity increased with $I(105)/I(110) = 0.26$, and FWHM of (104) peak = 0.184 (Table 3).

3.2.2. Isotope results

The initial isotopic composition of the "spiked proto-dolomite" was $\delta^{26}Mg = -2.00‰$ and $\delta^{25}Mg = 12.14‰$, which is 0.49‰ lower in $\delta^{26}Mg$, but 12.94‰ higher in $\delta^{25}Mg$, than the starting aqueous phase ("stock solution A") (Table 3). $\delta^{26}Mg$ values of the solid phase decreased by up to 0.5‰ after the exchange experiments, whereas

Table 3
Magnesium isotope and mineralogical parameters of samples in exchange experiments.

EXP. or Sample No.	Time (days)	Solution							Solid							Fractionation (solid-aq)						Dolomite XRD		
		$\delta^{26/24}$Mg	2SD	$\delta^{25/24}$Mg	2SD	$\delta^{26/25}$Mg	2SD	$n(N)$*	$\delta^{26/24}$Mg	2SD	$\delta^{25/24}$Mg	2SD	$\delta^{26/25}$Mg	2SD	$n(N)$*	$\Delta^{26/24}$Mg	2SD	$\Delta^{25/24}$Mg	2SD	$\Delta^{26/25}$Mg	2SD	$D(104)$	FWHM (104)	$I(105)$ / $I(110)$
Starting material "stock solution A"		−1.54	0.09	−0.79	0.05	−0.75	0.04	15(6)																
spiked proto-dolomite									−2.00	0.04	12.14	0.03	−13.99	0.02	7(2)							2.914	0.339	0.05
Exchange Exp.																								
Dex220	2	−1.48	0.02	−0.21	0.01	−1.28	0.03	3(1)	−2.21	0.01	0.06	0.01	−2.29	0.02	3(1)	−0.73	0.02	0.27	0.01	−1.01	0.03	2.891	0.213	0.46
	5	−1.42	0.03	−0.18	0.01	−1.25	0.03	3(1)	−2.18	0.04	−0.01	0.02	−2.18	0.02	3(1)	−0.76	0.05	0.17	0.02	−0.94	0.03	2.890	0.186	0.48
	12	−1.48	0.06	−0.17	0.01	−1.32	0.03	3(1)	−2.10	0.05	−0.04	0.05	−2.07	0.01	3(1)	−0.62	0.07	0.13	0.05	−0.75	0.03	2.890	0.189	0.45
Dex160	5	−1.52	0.07	−0.26	0.02	−1.26	0.03	3(1)	−2.38	0.02	1.39	0.02	−3.77	0.00	2(1)	−0.86	0.07	1.64	0.03	−2.51	0.03	2.900	0.191	0.28
	12	−1.55	0.05	0.11	0.01	−1.66	0.02	2(1)	−2.30	0.04	0.37	0.04	−2.68	0.01	2(1)	−0.75	0.06	0.26	0.04	−1.02	0.02	2.895	0.206	0.37
	22	−1.50	0.00	−0.19	0.00	−1.33	0.01	2(1)	−2.33	0.04	−0.35	0.02	−1.99	0.03	2(1)	−0.83	0.04	−0.16	0.02	−0.66	0.03	2.892	0.175	0.37
Dex130	1	−1.59	0.12	−0.80	0.07	−0.80	0.04	3(1)	−2.36	0.01	10.05	0.00	−12.30	0.01	3(1)	−0.78	0.12	10.85	0.07	−11.49	0.04	2.912	0.292	0.07
	3	−1.55	0.07	−0.74	0.01	−0.80	0.07	2(1)	−2.46	0.06	6.66	0.01	−9.07	0.03	2(1)	−0.91	0.09	7.41	0.02	−8.26	0.07	2.917	0.282	0.02
	9	−1.50	0.01	−0.71	0.01	−0.79	0.02	2(1)	−2.44	0.00	5.53	0.03	−7.93	0.01	2(1)	−0.94	0.01	6.24	0.03	−7.13	0.02	2.917	0.264	0.04
	20	−1.55	0.01	−0.39	0.04	−1.17	0.01	2(1)	−2.49	0.05	0.62	0.02	−3.11	0.01	2(1)	−0.93	0.05	1.01	0.05	−1.94	0.02	2.897	0.184	0.26
Total digestion	−1.58	0.03	−0.17	0.03	−1.43	0.01	2(1)																	

* n denotes total number of isotope analysis, N denotes number of replicates.

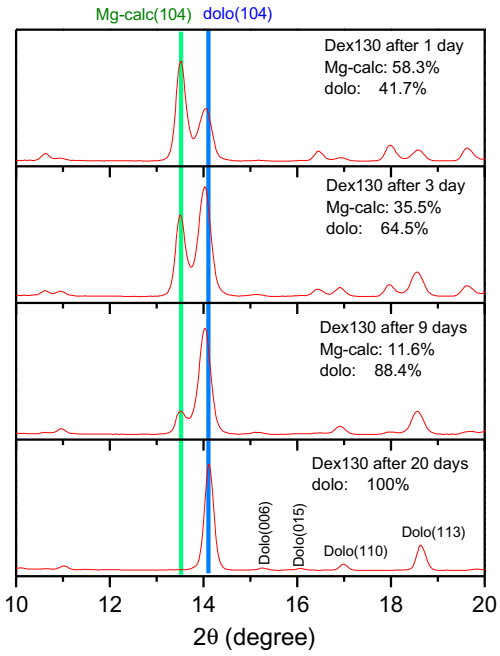

Fig. 6. XRD spectra of solid products in exchange experiment Dex130, showing the disappearance of the Mg-calcite (104) peak in the solid with increasing reaction time. Relative abundance of Mg-calcite and dolomite in solid was determined by Rietveld refinement of XRD spectrum between 5 and 40 degrees.

δ^{26}Mg values of the aqueous phase remained little changed (mostly around −1.4‰ to −1.5‰, Table 3), consistent with the high molar ratio of Mg between aqueous and solid phases (20:1 in initial reactants). Correspondingly, the apparent Mg isotope fractionation factor between solid and aqueous phases of the experiments ($\Delta^{26}Mg_{solid\text{-}aq}$) decreased from −0.49‰ at initial conditions, to ca. −0.76 to −0.62‰ for experiments at 220 °C, −0.86 to −0.75‰ for experiments at 160 °C, and −0.94 to −0.78‰ for experiments at 130 °C.

Exchange of the enriched-^{25}Mg tracer was documented by changes in δ^{25}Mg values for the solid phase, where, at 220 °C, δ^{25}Mg values decreased from 12.14‰ to −0.04‰ after 12 days, whereas δ^{25}Mg value of aqueous phase increased from −0.79‰ to −0.17‰ (Table 3). Change in δ^{25}Mg values was slower at 160 °C, where it took 12 days to decrease the δ^{25}Mg value of solid phase to 0.37‰ (Table 3). The change in δ^{25}Mg value of the solid in experiments at 130 °C was even slower, where it took 20 days to decrease the δ^{25}Mg value of solid to 0.62‰ (Table 3).

4. DISCUSSION

4.1. Reaction pathways of dolomitization

Dolomite was successfully synthesized by reacting a non-dolomite carbonate (aragonite, calcite, or nesquehonite) with a concentrated Mg–Ca solution. That dolomite was produced regardless of the starting carbonate material suggests that the experimental conditions (i.e., 1 M $MgCl_2$ +1 M $CaCl_2$ solution, temperature between 130 and 220 °C, and respective water saturation pressure) lay in a thermodynamically stable zone for dolomite, as has been suggested in previous studies (e.g., Rosenberg and Holland, 1964). Distinct starting materials produced distinct dolomite morphology (Fig. 1). In experiments that used calcite as the starting material, the dolomite crystal aggregates inherited the original calcite morphology, implying that dolomite formed through a mineral replacement process such as:

$$CaCO_3 + 0.5Mg^{2+} \rightarrow Ca_{0.5}Mg_{0.5}CO_3 + 0.5Ca^{2+} \quad (4)$$

In experiments that used aragonite or nesquehonite as the starting material, the dolomite did not retain the original carbonate morphology, but occurred as homogenous fine-grained crystals or their aggregates. These observations suggest that the dolomite crystals likely formed via a homogeneous precipitation mechanism such as:

$$0.5Ca^{2+} + 0.5Mg^{2+} + CO_3^{2-} \rightarrow Ca_{0.5}Mg_{0.5}CO_3 \quad (5)$$

where CO_3^{2+} was provided by decomposition of aragonite or nesquehonite:

$$CaCO_3 \rightarrow Ca^{2+} + CO_3^{2-} \quad (6)$$

$$MgCO_3 * 3H_2O \rightarrow Mg^{2+} + CO_3^{2-} + 3H_2O \quad (7)$$

The two mechanisms are physically consistent with the crystallographic features of dolomite and the three starting materials. Firstly, disordered dolomite, Mg-bearing calcite, and calcite share a common lattice configuration (space group: *R-3c*) despite differences in unit-cell volumes (Zhang et al., 2010), which facilitates cation replacement/exchange (Mg^{2+} for Ca^{2+}) for dolomitization of calcite, as shown in Eq. (4). Secondly, the unit-cell volume of calcite (367.8 Å^3) is larger than that of dolomite (319.4 Å^3), thus the mineral shrinks during replacement reaction, producing cavities, as shown in SEM images (Fig. 1, images B2 and B3). The cavities, in turn, serve as fluid channels that allow the reaction front to advance to inner portions of the calcite grains.

Aragonite has a radically different lattice configuration (space group: *Pcmn*) than that of dolomite, therefore aragonite does not serve as a template for dolomite growth. More importantly, because the unit-cell volume of aragonite (226.2 Å^3) is significantly smaller than that of dolomite (319.4 Å^3), the newly formed dolomite has to detach from its aragonite precursor during reaction due to lattice expansion. This explains the homogenous and fine-grained nature of dolomite produced from aragonite in the synthesis experiments (Fig. 1, images A2 and A3), where even aragonite crystals that were larger than 100 μm were converted to dolomite.

Nesquehonite has a unit-cell volume (501.2 Å^3) that is more than 50% larger than that of the dolomite. This volume difference likely explains the reason why dolomite did not retain the original rod-like crystal shape of nesquehonite (Fig. 1, image C2) in the experiments that used nesquehonite because replaced crystals would have collapsed with such a large proportion of voids. The initial $\Delta^{25}Mg_{solid\text{-}aq}$ and $\Delta^{26}Mg_{solid\text{-}aq}$ fractionations for the nesquehonite experiments did not show a natural mass-dependent behavior (i.e., $\Delta^{25}Mg_{solid\text{-}aq} \approx 0.521 * \Delta^{26}Mg_{solid\text{-}aq}$; Young and

Galy, 2004) because the starting solution was doped with a ^{25}Mg-enriched tracer. In the final products of the nesquehonite experiments, however, the $\Delta^{25}Mg_{solid\text{-}aq}$ and $\Delta^{26}Mg_{solid\text{-}aq}$ fractionations follow a mass-dependent behavior ($\Delta^{25}Mg_{solid\text{-}aq} \approx 0.521 * \Delta^{26}Mg_{solid\text{-}aq}$, Table 2), indicating complete mixing of Mg from the starting solution and nesquehonite before dolomite formation. A mechanistic understanding of the processes by which nesquehonite is converted to dolomite is hampered by the lack of time-series sampling for the nesquehonite experiments. Nevertheless, the fact that nesquehonite experiments formed spherical aggregates of dolomite crystals (Fig. 1, image C2) implies a kinetic-dominated process in a locally dolomite-saturated solution environment.

4.2. Recrystallization and ordering of dolomite

Significant changes occurred in both synthesis and exchange experiments in terms of recrystallization and ordering of dolomite. Morphological evidence for dolomite recrystallization includes coarsening of grain size over time (Fig. 1, images A2 and A3), disappearance of irregular crystal shapes, and development of rhombohedra crystal habit (Fig. 1, images D2 and D3), suggesting that recrystallization occurred via Ostwald ripening, or growth of larger crystals at the expense of dissolution of smaller crystals or crystals with defects that had high surface energy (Stoffregen et al., 1994; Li et al., 2011). Dolomite recrystallization was accompanied by significant, systematic, and inter-correlated changes in XRD features, including changes in $d(104)$ values and $I(105)/I(110)$ ratios (Fig. 3).

In addition to changes in morphology and lattice parameters observed in the hydrothermal experiments, the isotopic composition of dolomite systematically changed during recrystallization. In experiment series Arag160, disordered dolomite formed after 1 day of reaction and had an $^{87}Sr/^{86}Sr$ ratio distinct from that of the solution (Fig. 5). With increasing reaction time, however, $^{87}Sr/^{86}Sr$ ratios of solution and solid evolved to identical isotope compositions (Fig. 5), suggesting complete mixing/exchange between Sr in dolomite and aqueous solution. Such Sr isotope mixing/exchange was probably promoted by recrystallization via Ostwald ripening. In the isotope exchange experiments, starting dolomite was spiked with a ^{25}Mg tracer, and thus plots off a mass-dependent $\delta^{25}Mg$-$\delta^{26}Mg$ relation (Fig. 7). The $\delta^{25}Mg$ and $\delta^{26}Mg$ values of solid and aqueous phases for all three exchange experiments (Arag130, Arag160, Arag220) evolved toward a "secondary fractionation line" that goes through the $\delta^{25}Mg$-$\delta^{26}Mg$ mass balance of the system (Fig. 7). At complete isotope exchange, solid and aqueous phases would plot strictly on the "secondary fractionation line", and follow a mass-dependent fractionation relation of $\Delta^{25}Mg_{solid\text{-}aq} \approx 0.521 * \Delta^{26}Mg_{solid\text{-}aq}$ (e.g., Li et al., 2011). Fig. 7, therefore, demonstrates that a high degree of Mg isotope exchange occurred during exchange experiments, where exchange of Mg between dolomite and aqueous solution was probably promoted by recrystallization via Ostwald ripening.

4.3. Mg isotope fractionation between dolomite and aqueous solution

Our approach of using the "three isotope method" for determining stable isotope fractionation factors is well established across multiple isotope systems (e.g., Matsuhisa et al., 1978; Matthews et al., 1983; Shahar et al., 2008; Beard et al., 2010; Li et al., 2011, 2014), and potentially allows extrapolation to equilibrium fractionation factors at 100% exchange. There are two prerequisites, however, for a valid extrapolation with the "three isotope method", including: (1) no net mass transfer (i.e., net dissolution/precipitation) between the two phases, and (2) the instantaneous isotope fractionation factor remains constant during isotope exchange (i.e., no strong kinetic fractionations that are erased with time, or no additional phases involved in exchange). Prerequisite 1 ensures a fixed "100% exchange" target for extrapolation, and prerequisite 2 ensures a linear correlation between degree of isotope exchange and measured isotope fractionation, or a linear trajectory on a "three isotope" diagram (for two typical types of "three isotope" diagrams, see Matsuhisa et al., 1978 and Li et al., 2011) for a confident extrapolation to 100% exchange.

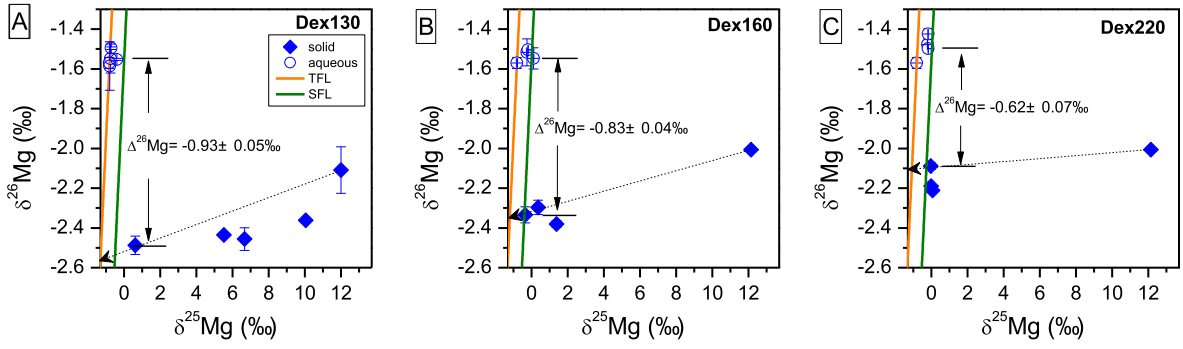

Fig. 7. Three isotope plot of the hydrothermal exchange experiments between ^{25}Mg enriched dolomite and normal Mg isotope composition aqueous Mg. TFL: terrestrial fractionation line for Mg, SFL: secondary fractionation line of Mg for this study. The fractionation factor and uncertainty in the plots are calculated from the longest duration experiment of the series (see Section 4.2). The dashed line with arrow is a reference line to show the trend of Mg isotope data for the solid phase from the beginning to the end of the experiment; it should be noted that this line is not used to extrapolate to 100% isotope exchange (see Section 4 in text).

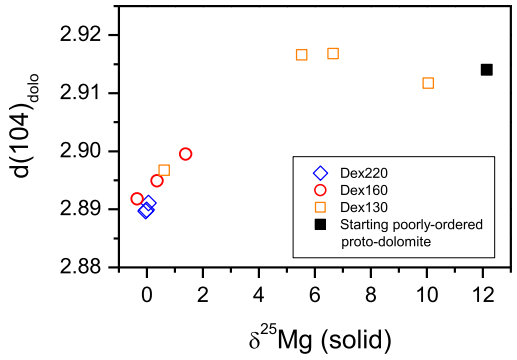

Fig. 8. Plot showing the positive correlation between $\delta^{25}Mg$ value of the solid and $d(104)$ value of dolomite in the exchange experiments.

For exchange experiment Dex130, Mg-calcite was produced and its abundance decreased with time (Fig. 6), which violates prerequisites 1 of the "three isotope method" for extrapolation. On the other hand, the positive correlation between $\delta^{25}Mg_{solid}$ and $d(104)$ of dolomite for the exchange experiments (Fig. 8) indicates that the lattice configuration of dolomite changed during recrystallization and isotopic exchange. Because bonding conditions affects equilibrium Mg isotope fractionation factors for minerals (Schauble, 2004; Li et al., 2014), the change in $d(104)$ of dolomite during exchange experiments might indicate a drifting instantaneous isotope fractionation factor between solid and aqueous phases, thus violating prerequisite 2 of "three isotope method". On the "three isotope plot" for experiment Dex130, therefore, the data points for the time series experiments do not plot along a straight line (Fig. 7).

Despite these issues discussed above, where complex temporal changes in Mg isotope fractionations occurred, the very high degree of Mg isotope exchange attained at the end of these exchange experiments allows an estimation of the Mg isotope fractionation factor. The degree of isotope exchange (F) can be defined by the following equation:

$$F = (\Delta^{25}Mg_t - \Delta^{25}Mg_i)/(\Delta^{25}Mg_e - \Delta^{25}Mg_i) \quad (8)$$

where $\Delta^{25}Mg_t$ is the difference in $\delta^{25}Mg$ values between the solid and aqueous pair at a given time t ($\delta^{25}Mg_{solid}$-$\delta^{25}Mg_{aq}$, or $\Delta^{25}Mg_{solid\text{-}aq}$), and $\Delta^{25}Mg_i$ and $\Delta^{25}Mg_e$ are the initial and equilibrium $\Delta^{25}Mg_{solid\text{-}aq}$ values, respectively. This function is similar to that previously proposed (Johnson et al., 2002; Li et al., 2011), but because F is not cast in terms of a single phase, it is less sensitive to complexities produced by net mass transfer. $\Delta^{25}Mg_e$ fractionations are estimated at −0.3‰, −0.4‰ and −0.5‰ at 220 °C, 160 °C, and 130 °C, respectively, based on apparent fractionation factors obtained from the synthesis experiments, and the mass-dependent relation (i.e., $\Delta^{25}Mg_e = 0.521 * \Delta^{26}Mg_e$). Based on equation (8), the degree of isotope exchange is 96.7% for exp. Dex220 after 12 days, 98.2% for exp. Dex160 after 22 days, and 88.8% for exp. Dex130 after 20 days. The differences in $\delta^{26}Mg$ values between dolomite and aqueous solution pairs ($\Delta^{26}Mg_{dolo\text{-}aq}$) at the end of exchange experiments, therefore, provide estimates for equilibrium Mg isotope fractionation factors for ordered dolomite, which are −0.62 ± 0.07‰ at 220 °C, −0.83 ± 0.04‰ at 160 °C, and −0.93 ± 0.05‰ at 130 °C (Table 3).

It is important to note that the $\Delta^{26}Mg_{dolo\text{-}aq}$ fractionation factors derived from the exchange experiments at 220 and 160 °C are consistent with the respective $\Delta^{26}Mg_{dolo\text{-}aq}$ fractionations inferred from the last sampled time-series synthesis experiments, and are independent of the starting material. As shown in Fig. 4, the apparent $\Delta^{26}Mg_{dolo\text{-}aq}$ fractionation factors evolved during the time-series synthesis experiments. In general, experiments with the longest duration have the highest probability for approaching equilibrium, and this is supported by the XRD data that show the degree of ordering in dolomite improves with time in each time-series experiment (Fig. 3). The *best estimates* of equilibrium fractionation factors therefore can be calculated by combining results from exchange experiments and the last $\Delta^{26}Mg_{dolo\text{-}aq}$ fractionation data point of each time-series synthesis experiment (Arag220, Arag160, and Calc220). Using Isoplot® (Ludwig, 1999), the weighted average $\Delta^{26}Mg_{dolo\text{-}aq}$ fractionation at 220 °C is calculated to be −0.65 ± 0.04‰ (95% confidence, $n = 3$, MSWD = 1.18, combining Dex220, Arag220@day13, and Calc220@day13), and the weighted average $\Delta^{26}Mg_{dolo\text{-}aq}$ fractionation at 160 °C is calculated to be −0.84 ± 0.04‰ (95% confidence, $n = 2$, MSWD = 1.05, combining Dex160 and Arag160@day52). The close correspondence between the exchange and synthesis experiment results suggests that our inferred final fractionation factors are pathway independent, and therefore can be considered equilibrium fractionation factors. The consistency between $\Delta^{26}Mg_{solid\text{-}aq}$ fractionation factors from synthesis experiments and exchange experiments at 130 °C is poorer relative to those at higher temperatures. Part of this discrepancy is probably a result of the fact that the solid phases in the synthesis experiments at 130 °C were not pure dolomite (Table 1). Therefore, only the $\Delta^{26}Mg_{dolo\text{-}aq}$ fractionation (−0.93 ± 0.05‰, 2SD, or 95% confidence) of the last sampled Dex130 experiment (88.8% exchange, and pure dolomite in solid phase) was taken as the equilibrium fractionation factor.

It is evident that the magnitude of Mg isotope fractionation between dolomite and aqueous solution decreases with increasing temperature, which is consistent with first-principles of isotope fractionation, where a linear correlation between isotope fractionation and $1/T^2$ is expected (Bigeleisen and Mayer, 1947; Urey, 1947; O'Neil, 1986; Schauble, 2004). The temperature-dependent function for Mg isotope fractionation between dolomite and aqueous solution, therefore, is obtained by regression of experimentally-derived $\Delta^{26}Mg_{dolo\text{-}aq}$ data at different temperatures (Fig. 9):

$$\Delta^{26}Mg_{dolo\text{-}aq} = -0.1554(\pm 0.0096) \times 10^6/T^2 \quad (9)$$

where T is in Kevin (K). Note that this equation is forced through a zero intercept to be consistent with a zero fractionation at infinite temperature, and this approach has been commonly used in experimental studies of isotope fractionation factors (e.g., Young et al., 2015; and references therein).

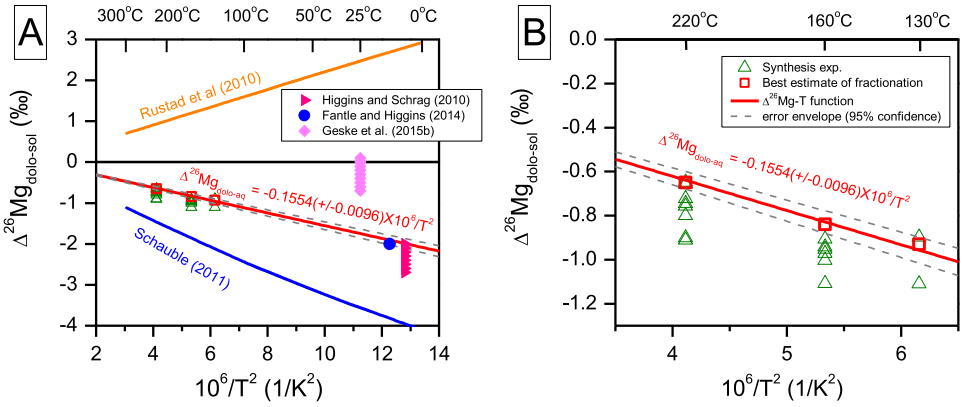

Fig. 9. (A) Experimentally determined Δ^{26}Mg-temperature fractionation functions, and comparison with previous theoretical calculations (Rustad et al., 2010; Schauble 2011) and natural system investigations (Higgins and Schrag, 2010; Fantle and Higgins, 2014; Geske et al., 2015b). The T-Δ^{26}Mg function with 95% confidence envelope shown for the results of this study is calculated using Origin® software, by fitting the three best estimate fractionation factors at temperatures of 130, 160, and 220 °C and forcing the best fitting line through a zero intercept at infinite temperature. (B) Detailed plot of experimental data and regression line at temperatures of 130, 160, and 220 °C. The spread in synthesis data most likely reflects isotopic effect of lattice ordering. For more details of the time series synthesis experiments, see Fig. 4; for details about how the best estimate of fractionation was obtained for each temperature, see discussions in Section 4.3.

In the time-series synthesis experiments (Arag160, Arag220), $\Delta^{26}Mg_{dolo\text{-}aq}$ fractionations suggest evolution toward fractionations for ordered dolomite that are up to 0.25‰ higher than those of synthesized disordered dolomite (Fig. 4; Fig. 9). This contrast is unlikely to reflect kinetic isotope effects, which would shift $\Delta^{26}Mg_{min\text{-}aq}$ fractionations toward more positive values (Immenhauser et al., 2010; Mavromatis et al., 2013). Instead, the lower $\Delta^{26}Mg_{dolo\text{-}aq}$ fractionations in the early stage of the synthesis experiments may reflect crystal chemical effects on isotopic fractionation, as the early products are disordered dolomite and later products are ordered dolomite (see Section 4.2). Disordered dolomite has higher $d(104)$ values (Table 2), thus longer average Mg–O bond length than ordered dolomite. It has been shown that, given the same coordination environment, minerals that have shorter Mg–O bond length have a higher affinity for heavier Mg isotopes, thus higher $\Delta^{26}Mg_{min\text{-}aq}$ fractionation (Li et al., 2014). Bond length difference, therefore, is a plausible explanation for the inferred differences in $\Delta^{26}Mg_{dolo\text{-}aq}$ fractionations between disordered dolomite and ordered dolomite.

4.4. Comparison with previous studies

Equilibrium fractionation factors of Mg isotopes between dolomite and aqueous solution have been calculated in two independent studies by Rustad et al. (2010) and Schauble (2011). Rustad et al. (2010) predicted positive $\Delta^{26}Mg_{dolo\text{-}aq}$ fractionations, whereas Schauble (2011) predicted negative $\Delta^{26}Mg_{dolo\text{-}aq}$ fractionations (Fig. 9). Experimentally calibrated fractionation factors for dolomite from this study lie between the two predictions, but are most consistent with Schauble (2011) (Fig. 9). A detailed discussion on the origin of the discrepancy between the calculations of Rustad et al. (2010) and Schauble (2011) is beyond the scope of this paper, although we note that the modeling of dolomite by Rustad et al. (2010) is based on a cluster model, whereas the modeling of dolomite by Schauble (2011) is based on a phonon model. It is important to note that both Rustad et al. (2010) and Schauble (2011) treated Mg^{2+} ions as an infinitely diluted species in water, which may not be an adequate approximation for our experiments. Indeed, high concentrations of Mg^{2+} and Ca^{2+} are a requirement for precipitation of dolomite in almost all dolomite genesis models (e.g., Warren, 2000). In this study, dolomite generally precipitated from a solution of 1 M $MgCl_2$ and 1 M $CaCl_2$, which has molar ratios of 1:1:4:50 for Mg:Ca:Cl:H_2O. Because each of the first hydration shells of Mg^{2+}, Ca^{2+}, and Cl^- are comprised of 6 water molecules, and the second hydration shell of Mg^{2+} comprises of 12 water molecules (Ohtaki and Radnai, 1993), there are not enough water molecules to satisfy the second hydration shell for all the hydrated ions (only 14 mol of non-first shell water for 1 mol of $MgCl_2$ and 1 mol of $CaCl_2$). Competition for second shell waters in a high salt content solution, therefore, likely results in interaction of hydrated ions with the second hydration shell of any Mg^{2+}, although direct Mg–Cl pairing is unlikely to exist under the solution condition of this study (Callahan et al., 2010). Differences in solvation of Mg^{2+} ion potentially affect Mg isotope fractionation, as implied by the modeling of Rustad et al. (2010). Isotopic effects of high concentration salt have been reported for O isotopes (e.g., Sofer and Gat, 1972; Horita et al., 1993; Hu and Clayton, 2003), where ~1‰ offset in $\Delta^{18}O$ fractionations can be produced by 1 mol of dissolved $MgCl_2$ or $CaCl_2$ at ambient temperatures (Sofer and Gat, 1972; Horita et al., 1993). Whether salt effects also exist for Mg isotopes is a topic that should be explored by future theoretical and experimental studies.

A number of workers have measured Mg isotope compositions of natural dolomite samples, which allow estimation of $\Delta^{26}Mg_{dolo\text{-}aq}$ fractionations from some

low-temperature settings. Geske et al. (2015b) analyzed modern Sabkha dolomite and related pore water from the Gulf region and obtained a $\Delta^{26}Mg_{dolo\text{-}aq}$ fractionation factor range of -0.7‰ to +0.1‰ (Fig. 9). Higgins and Schrag (2010) analyzed Mg isotope compositions of pore water and dolomite from three ODP drill cores, and based on reactive transport modeling, Higgins and Schrag (2010) concluded that a $\Delta^{26}Mg_{dolo\text{-}aq}$ fractionation factor of $-2.0‰$ to $-2.7‰$ is needed to explain the vertical profile of $\delta^{26}Mg$ values of pore water and dolomite. Similar conclusions have been drawn in a more recent study on another ODP site, where a $\Delta^{26}Mg_{dolo\text{-}aq}$ fractionation factor of $-2.0‰$ is deduced from modeling of the observed $\delta^{26}Mg$ values along the drill core (Fantle and Higgins, 2014). It should be noted that the ODP drill core studied by Fantle and Higgins (2014) comes from a tropical platform environment, where temperature (7.5–17.5 °C, average 12.5 °C) is higher than the ocean bottom (estimated $T = 4$ °C) drill cores studied by Higgins and Schrag (2010). In addition, the dolomite in drill cores study by Higgins and Schrag (2010) is related to methanogenesis, whereas the dolomite in ODP drill core studied by Fantle and Higgins (2014) is not. These two factors might explain the slight difference in $\Delta^{26}Mg_{dolo\text{-}aq}$ fractionation factor between the two ODP studies. Nevertheless, the $\Delta^{26}Mg_{dolo\text{-}aq}$ fractionation factors obtained from modeling of ODP drill cores are consistent with the T-$\Delta^{26}Mg$ function for dolomite in this study (Fig. 9), although we note that the extrapolation from hydrothermal temperatures to surface temperatures on a $1/T^2$ scale is large, and more experimental work at lower temperatures is needed to better constrain the $\Delta^{26}Mg$ fractionation at low temperatures.

4.5. Potential applications

Determination of the dolomite-fluid Mg isotope fractionation factors provide important constraints for interpreting the Mg isotope variations in natural dolomite. The isotopic composition of Mg ($\delta^{26}Mg$) in seawater is controlled by a balance between the sources and sinks of Mg and their isotopic compositions, one of which is the dolomite Mg flux. Below we illustrate the sensitivity of the dolomite-fluid Mg isotope fractionation factor to modeling ancient seawater Mg cycling, as well as application to understanding the origin of hydrothermal dolomite, which provides a broader context for the experimental results discussed above.

4.5.1. Sedimentary dolomite and global Mg cycling over geological time

Tipper et al. (2006) proposed a simplified steady-state function ($\delta_{riv}\boldsymbol{J}_{riv} = \delta_{hyd}\boldsymbol{J}_{hyd} + \delta_{carb}\boldsymbol{J}_{carb}$) to constrain the oceanic cycling of Mg using Mg isotopes, where δ_{riv}, δ_{hyd}, and δ_{carb} are Mg isotope compositions of riverine input, hydrothermal output, and output flux by carbonate precipitation (mainly dolomitization), respectively, and $\boldsymbol{J}$ represents the fluxes for each of the inputs and outputs. Based on compilation of mass-age data for sedimentary carbonate in the Phanerozoic, Wilkinson and Algeo (1989) proposed a curve for the relative proportion of river Mg removed by marine dolomitization ($\boldsymbol{J}_{dolo}$) versus hydrothermal alteration at mid-ocean ridge ($\boldsymbol{J}_{hyd}$) over the past 560 Ma (Fig. 10). Using the Mg flux ratios of Wilkinson and Algeo (1989), it is possible to reconstruct the global Mg cycling history and the Mg isotope record based on the steady-state function of Tipper et al. (2006), if δ_{riv}, δ_{hyd}, and δ_{carb} can be defined. For simplicity, we assume a constant riverine input over the Phanerozoic ($\delta_{riv} = -1.1‰$; Tipper et al., 2006). Based on the experimentally derived $\Delta^{26}Mg$-temperature function determined in this study, we

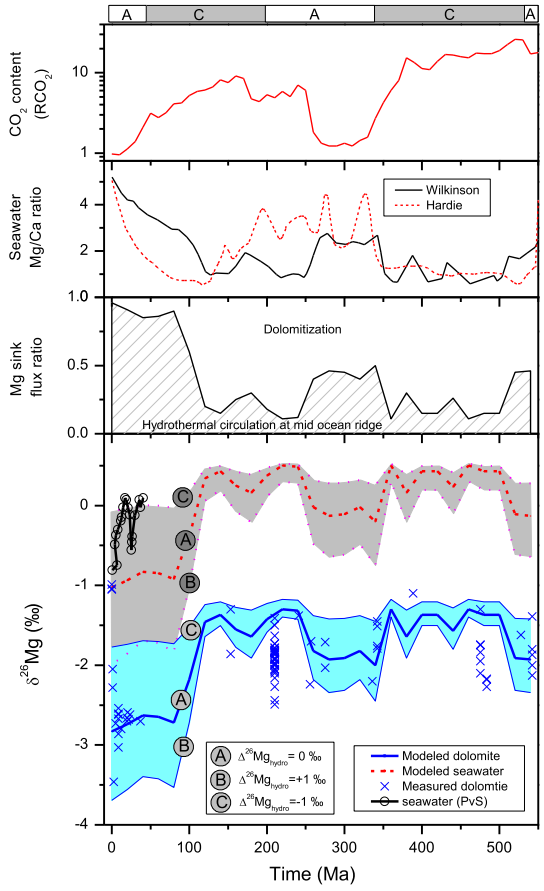

Fig. 10. Correlations between (from bottom to top) modeled Mg isotope compositions of seawater and sedimentary dolomite in the past 560 Ma, and previously proposed Mg sink flux ratio (Wilkinson and Algeo, 1989), seawater Mg/Ca molar ratio (Wilkinson and Algeo, 1989; Hardie, 1996), atmospheric CO_2 (relative to modern value; Berner and Kothavala, 2001), and seawater primary carbonate mineralogy (A: aragonite sea, C: calcite sea; Sandberg, 1983) over the Phanerozoic. For comparison, a $\delta^{26}Mg$ curve for seawater (PvS) in the past 40 Ma suggested by Pogge von Strandmann et al. (2014) and Mg isotope compositions of Phanerozoic sedimentary dolomite reported by Azmy et al. (2013), Fantle and Higgins (2014), Geske et al. (2012, 2015a), Higgins and Schrag (2010), Jacobson et al. (2010), and Mavromatis et al. (2014) are plotted with the model results. The model assumes a constant Mg isotope fractionation factor between dolomite and aqueous solution, but different Mg isotope fractionation during hydrothermal uptake of seawater at mid-ocean ridges ($\Delta^{26}Mg_{hydro} = 0‰$, $+1‰$, $-1‰$), and the modeling results are denoted by symbols A, B, and C, respectively.

set a constant Mg isotope fractionation factor during dolomitization ($\delta_{carb} = \delta_{dolo} = \delta_{seawater} - 1.8‰$; $T \approx 20$ °C). There is uncertainty in Mg isotope composition of the Mg flux (δ_{hyd}) removed by hydrothermal circulation at mid ocean ridges, because low-temperature circulation at flanks of mid-ocean ridge is an important sink for Mg (Mottl and Wheat, 1994; Elderfield and Schultz, 1996). At high temperatures, Mg sequestration in hydrothermal systems is assumed to be quantitative, resulting in a zero solid–fluid fractionation factor (Tipper et al., 2006), but such an assumption may not be valid at low temperatures. To address this issue, we assumed three different fractionation factors ($\Delta^{26}Mg_{hydro} = \delta_{seawater}$-$\delta_{hyd} = -1‰$, 0‰, +1‰) between seawater and hydrothermal sink. Based on these input parameters, we calculate the model-based δ^{26}Mg curves for sedimentary dolomite, and seawater in the Phanerozoic, which are shown in Fig. 10.

Comparison of the reported Mg isotope data of natural dolomite with the modeled δ^{26}Mg curve for dolomite shows a first-order degree agreement, despite scatter in natural data (Fig. 10). In particular, the modeled δ^{26}Mg curve reproduces the observed drop in δ^{26}Mg for dolomite in the Cenozoic, and this mirrors the decrease in dolomitization intensity in the Cenozoic sedimentary records (Fig. 10). It is shown in Fig. 10 that differences in assumptions of $\Delta^{26}Mg_{hydro}$ fractionation can significantly affect the modeled δ^{26}Mg values for seawater and sedimentary if $\boldsymbol{J}_{hyd}$ flux is greater than $\boldsymbol{J}_{carb}$ flux, but it seems that when $\Delta^{26}Mg_{hydro}$ fractionation is set to close to zero, there is the best agreement between modeled and measured δ^{26}Mg data for Cenozoic dolomite. Regardless of the uncertainty in Mg isotope fractionation during hydrothermal activity at mid-ocean ridges, the modeled curves for seawater and dolomite δ^{26}Mg values show sensitive response to changes in dolomitization intensity, and broadly correlate with atmospheric CO_2 levels and seawater Mg/Ca ratios over the Phanerozoic (Fig. 10), suggesting Mg isotopes could be an useful tool to study global Mg cycling.

Because the model presented in Fig. 10 is based on a number of assumptions, discrepancy between modeled and measured data implies inconsistency between model assumptions and natural processes. Notably, modern or young Sabkha dolomite samples (Azmy et al., 2013; Geske et al., 2015b) generally have δ^{26}Mg values that are higher than the model curve (with $\Delta^{26}Mg_{hydro} = 0‰$), but some fossil Sabkha dolomite such as the upper Triassic Hauptdolomit Formation (Geske et al., 2012) and mixing zone dolomite such as the Lower Ordovician St. George Group (Azmy et al., 2013) has δ^{26}Mg values lower than the model curve (Fig. 10). The apparent Mg isotope fractionation factors derived from modern Sabkha environment vary between −0.7‰ and +0.1‰ (Geske et al., 2015b), which are significantly higher than the equilibrium isotope fractionation factor for dolomite based on this study (Fig. 9A), suggesting that equilibrium Mg isotope fractionation is not applicable during early dolomitization in some Sabkha environments. The decrease in δ^{26}Mg values of older fossil Sabkha dolomite has been interpreted to reflect post-depositional diagnetict resetting by Geske et al. (2015a), who emphasized the importance of screening samples before using them to interpret Mg global cycling. The Lower Ordovician St. George Group (Azmy et al., 2013) have δ^{26}Mg values lower than the model curve, which is consistent with a "mixing zone" origin (Azmy et al., 2008; Conliffe et al., 2012), where Mg source for dolomite came from a mixture of riverine input and seawater, which had δ^{26}Mg values lower than the modeled seawater, but higher than −1.1‰ (Fig. 10). In addition, Pogge von Strandmann et al. (2014) suggested a δ^{26}Mg curve for seawater in the past 40 Ma based on foraminifera records. According to Pogge von Strandmann et al. (2014), the seawater δ^{26}Mg ocillated between −0.8‰ and 0‰ in the recent 40 Ma, but such significant recent ocillation in seawater δ^{26}Mg is absent in the modeling results of this study. Pogge von Strandmann et al. (2014) explained the significant seawater δ^{26}Mg change by combination of changes in riverine input and dolomitization intensity in the last 40 m.y.; in contrast, riverine input is set to be constant in the model shown in Fig. 10, and the dolomitization intensity has changed little in the last 40 m.y. according to the calculation of Wilkinson and Algeo (1989). To summarize, with the Mg isotope fractionation factors constrained, it is now possible to further explore the questions of global Mg cycling by combination of models and natural sample analyses.

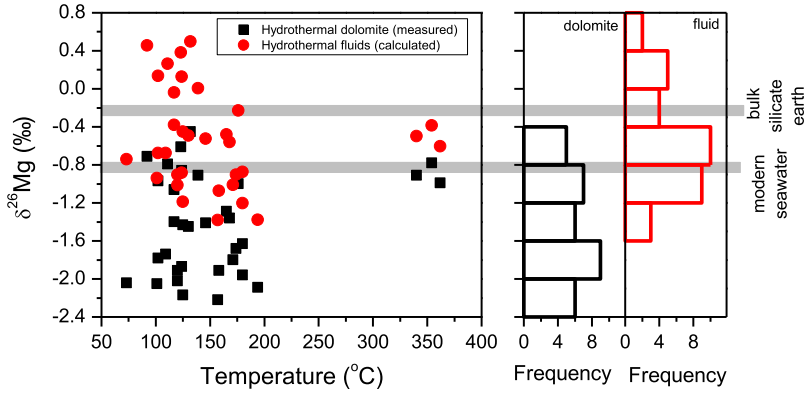

Fig. 11. Plot of δ^{26}Mg values of hydrothermal dolomite against temperature, and the respective δ^{26}Mg values for hydrothermal fluid, calculated using the Δ^{26}Mg-temperature function in this study. Histogram for the δ^{26}Mg values of dolomite and fluids are shown to the right of the plot. δ^{26}Mg and temperature data for hydrothermal dolomite are compiled from studies of Azmy et al. (2013), Lavoie et al. (2014), and Geske et al. (2015a,b).

4.5.2. Dolomitization at hydrothermal conditions

Hydrothermal dolomite is also an important type of dolomite, which is commonly found in deep burial diagenesis of sedimentary carbonates, and hydrothermal mineral deposits such as skarn-type deposits, and Mississippi Valley-type (MVT) Zn–Pb deposits. A number of studies (Azmy et al., 2013; Lavoie et al., 2014; Geske et al., 2015a) have reported Mg isotope compositions of hydrothermal dolomite, together with precipitation temperatures obtained by fluid inclusion or Δ_{47} clumped isotope geothermometry. These data are compiled in Fig. 11, together with the δ^{26}Mg values for the hydrothermal fluids calculated using the experimentally calibrated $\Delta^{26}Mg_{dolo\text{-}aq}$ -T function of this study. Fig. 11 shows that the δ^{26}Mg values calculated for hydrothermal fluids range between $-1.3‰$ and $+0.5‰$. A large proportion of the hydrothermal fluid δ^{26}Mg values are above the modern seawater value of $-0.8‰$ (Ling et al., 2011), some are even above the bulk silicate earth value of $-0.2‰$ to $-0.3‰$ (Teng et al., 2010), which implies that the Mg source for hydrothermal fluids could reflect earlier dolomite precipitation that removed isotopically light Mg from solution. The low δ^{26}Mg values would suggest that the hydrothermal fluid could have originated from a low-δ^{26}Mg source such as sedimentary dolomite, followed by extensive remobilization at elevated temperature (less negative $\Delta^{26}Mg_{dolo\text{-}aq}$ fractionation). Such low δ^{26}Mg values would indicate little dolomite precipitation. The wide range in calculated δ^{26}Mg values for hydrothermal fluids, particularly those <200 °C, suggests that stable Mg isotopes may be a sensitive tracer of fluid-rock interaction histories in Mg-bearing systems.

5. CONCLUSION

We successfully synthesized dolomite at hydrothermal conditions using aragonite, calcite, and nesquehonite as starting materials, allowing tests of the pathway dependence of Mg isotope fractionation. The morphology of synthesized dolomite is dependent on the mineralogy of starting minerals, suggesting different pathways of dolomite precipitation. Initially, synthesized dolomite occurred as fine-grained disordered dolomite but with time it recrystallized to coarser-grained ordered dolomite. In addition to synthesis approaches, isotope exchange was evaluated using $^{87}Sr/^{86}Sr$ isotopes and enriched ^{25}Mg isotope tracers, and these showed near-complete isotope exchange between dolomite and aqueous solutions at the end of most of the hydrothermal experiments.

Magnesium isotope fractionation factors between dolomite and aqueous solutions obtained from synthesis and exchange experiments converged with time and were independent of dolomite morphology, suggesting attainment of isotopic equilibrium. Combining results from synthesis experiments and exchange experiments, the $\Delta^{26}Mg_{dolo\text{-}aq}$ fractionation for ordered dolomite is estimated at $-0.65 \pm 0.04‰$ (95% confidence, $n = 3$, MSWD = 1.18), $-0.84 \pm 0.04‰$ (95% confidence, $n = 2$, MSWD = 1.05), and $-0.93 \pm 0.05‰$ (2SD, or 95% confidence) at 220, 160, and 130 °C, respectively. These results define a temperature-fractionation function for Mg in ordered dolomite:

$$\Delta^{26}Mg_{dolo\text{-}aq} = -0.1554(\pm 0.0096) \times 10^6/T^2$$

where T is in Kelvin. Furthermore, experiments in this study suggest that disordered dolomite has $\Delta^{26}Mg_{dolo\text{-}aq}$ fractionation factors up to $0.25‰$ lower than the ordered dolomite at temperatures of 160–220 °C, and this is attributed to longer Mg–O bonds in disordered dolomite. The experimentally calibrated $\Delta^{26}Mg_{dolo\text{-}aq}$ fractionation factors lie between those calculated by Schauble (2011) and Rustad et al. (2010). $\Delta^{26}Mg_{dolo\text{-}aq}$ fractionations extrapolated to low temperatures using the Δ^{26}Mg-T function of this study match well with $\Delta^{26}Mg_{dolo\text{-}aq}$ fractionation factors obtained by modeling of Mg isotope compositions of ODP drill core samples.

This study shows that significant Mg isotope fractionation occurs during dolomite precipitation and that extensive dolomitization over geological history could have significantly influenced the Mg isotope composition of seawater that could be preserved in massive syndepositional dolostones. At a local scale, Mg isotopes may be useful to trace evolution and migration of hydrothermal fluids where hydrothermal dolomite were formed. Magnesium isotopes in dolomite, therefore, have significant potential in studies of past seawater chemistry, Mg global cycling, and hydrothermal processes.

ACKNOWLEDGMENTS

This paper benefited from discussions with Or Bialik, Fangfu Zhang and Zhizhang Shen, and constructive comments from John Higgins and Josh Wimpenny, as well as editorial comments by Jeff Alt. This study was supported by the NASA Astrobiology Institute of United States. W. Li is supported by the National Science Foundation of China (41473002).

APPENDIX A. SUPPLEMENTARY DATA

Supplementary data associated with this article can be found, in the online version, at http://dx.doi.org/10.1016/j.gca.2015.02.024.

REFERENCES

Azmy K., Lavoie D., Knight I. and Chi G. (2008) Dolomitization of the Lower Ordovician Aguathuna formation carbonates, Port au Port Peninsula, western Newfoundland, Canada: implications for a hydrocarbon reservoir. *Can. J. Earth Sci.* **45**, 795–813.

Azmy K., Lavoie D., Wang Z., Brand U., Al-Aasm I., Jackson S. and Girard I. (2013) Magnesium-isotope and REE compositions of Lower Ordovician carbonates from eastern Laurentia: implications for the origin of dolomites and limestones. *Chem. Geol.* **356**, 64–75.

Beard B. L., Handler R. M., Scherer M. M., Wu L., Czaja A. D., Heimann A. and Johnson C. M. (2010) Iron isotope fractionation between aqueous ferrous iron and goethite. *Earth Planet. Sci. Lett.* **295**, 241–250.

Beard B. L., Ludois J. M., Lapen T. J. and Johnson C. M. (2013) Pre-4.0 billion year weathering on Mars constrained by Rb–Sr geochronology on meteorite ALH84001. *Earth Planet. Sci. Lett.* **361**, 173–182.

Berner R. A. and Kothavala Z. (2001) Geocarb III: a revised model of atmospheric CO2 over phanerozoic time. *Am. J. Sci.* **301**, 182–204.

Bigeleisen J. and Mayer M. G. (1947) Calculation of equilibrium constants for isotopic exchange reactions. *J. Chem. Phys.* **15**, 261–267.

Burns S. J., McKenzie J. A. and Vasconcelos C. (2000) Dolomite formation and biogeochemical cycles in the Phanerozoic. *Sedimentology* **47**, 49–61.

Callahan K. M., Casillas-Ituarte N. N., Roeselová M., Allen H. C. and Tobias D. J. (2010) Solvation of magnesium dication: molecular dynamics simulation and vibrational spectroscopic study of magnesium chloride in aqueous solutions. *J. Phys. Chem. A* **114**, 5141–5148.

Conliffe J., Azmy K. and Greene M. (2012) Dolomitization of the lower Ordovician Catoche formation: Implications for hydrocarbon exploration in western Newfoundland. *Mar. Pet. Geol.* **30**, 161–173.

Elderfield H. and Schultz A. (1996) Mid-ocean ridge hydrothermal fluxes and the chemical composition of the ocean. *Ann. Rev. Earth Planet. Sci.* **24**, 191–224.

Fantle M. S. and Higgins J. (2014) The effects of diagenesis and dolomitization on Ca and Mg isotopes in marine platform carbonates: Implications for the geochemical cycles of Ca and Mg. *Geochim. Cosmochim. Acta* **142**, 458–481.

Fischer A. G. (1984) The two Phanerozoic supercycles. In *Catastrophies in Earth History* (eds. W. A. Berggren and J. A. Vancouvering). Princeton University Press, Princeton, pp. 129–148.

Galy A., Yoffe O., Janney P. E., Williams R. W., Cloquet C., Alard O., Halicz L., Wadhwa M., Hutcheon I. D., Ramon E. and Carignan J. (2003) Magnesium isotope heterogeneity of the isotopic standard SRM980 and new reference materials for magnesium-isotope-ratio measurements. *J. Anal. At. Spectrom.* **18**, 1352–1356.

Geske A., Zorlu J., Richter D. K., Buhl D., Niedermayr A. and Immenhauser A. (2012) Impact of diagenesis and low grade metamorphosis on isotope (δ^{26}Mg, δ^{13}C, δ^{18}O and ^{87}Sr/^{86}Sr) and elemental (Ca, Mg, Mn, Fe and Sr) signatures of Triassic sabkha dolomites. *Chem. Geol.* **332–333**, 45–64.

Geske A., Goldstein R. H., Mavromatis V., Richter D. K., Buhl D., Kluge T., John C. M. and Immenhauser A. (2015a) The magnesium isotope (δ^{26}Mg) signature of dolomites. *Geochim. Cosmochim. Acta* **149**, 131–151.

Geske A., Lokier S., Dietzel M., Richter D. K., Buhl D. and Immenhauser A. (2015b) Magnesium isotope composition of sabkha porewater and related (Sub-)Recent stoichiometric dolomites, Abu Dhabi (UAE). *Chem. Geol.* **393–394**, 112–124.

Given R. K. and Wilkinson B. H. (1987) Dolomite abundance and stratigraphic age; constraints on rates and mechanisms of Phanerozoic dolostone formation. *J. Sediment. Res.* **57**, 1068–1078.

Graf D. L. and Goldsmith J. R. (1956) Some Hydrothermal Syntheses of Dolomite and Protodolomite. *J. Geol.* **64**, 173–186.

Hardie L. A. (1996) Secular variation in seawater chemistry: An explanation for the coupled secular variation in the mineralogies of marine limestones and potash evaporites over the past 600 m.y. *Geology* **24**, 279–283.

Higgins J. A. and Schrag D. P. (2010) Constraining magnesium cycling in marine sediments using magnesium isotopes. *Geochim. Cosmochim. Acta* **74**, 5039–5053.

Holland H. D. (2005) Sea level, sediments and the composition of seawater. *Am. J. Sci.* **305**, 220–239.

Horita J., Wesolowski D. J. and Cole D. R. (1993) The activity-composition relationship of oxygen and hydrogen isotopes in aqueous salt solutions: I. Vapor-liquid water equilibration of single salt solutions from 50 to 100 °C. *Geochim. Cosmochim. Acta* **57**, 2797–2817.

Hu G. and Clayton R. N. (2003) Oxygen isotope salt effects at high pressure and high temperature and the calibration of oxygen isotope geothermometers. *Geochim. Cosmochim. Acta* **67**, 3227–3246.

Immenhauser A., Buhl D., Richter D., Niedermayr A., Riechelmann D., Dietzel M. and Schulte U. (2010) Magnesium-isotope fractionation during low-Mg calcite precipitation in a limestone cave – Field study and experiments. *Geochim. Cosmochim. Acta* **74**, 4346–4364.

Jacobson A. D., Zhang Z., Lundstrom C. and Huang F. (2010) Behavior of Mg isotopes during dedolomitization in the Madison Aquifer, South Dakota. *Earth Planet. Sci. Lett.* **297**, 446–452.

Johnson C. M., Skulan J. L., Beard B. L., Sun H., Nealson K. H. and Braterman P. S. (2002) Isotopic fractionation between Fe(III) and Fe(II) in aqueous solutions. *Earth Planet. Sci. Lett.* **195**, 141–153.

Kaczmarek S. E. and Sibley D. F. (2011) On the evolution of dolomite stoichiometry and cation order during high-temperature synthesis experiments: an alternative model for the geochemical evolution of natural dolomites. *Sed. Geol.* **240**, 30–40.

Katz A. and Matthews A. (1977) The dolomitization of CaCO3: an experimental study at 252–295 °C. *Geochim. Cosmochim. Acta* **41**, 297–308.

Komareneni S., Freeborn W. P. and Smith C. A. (1979) Simple cold-weld sealing of noble-metal tubes. *Am. Mineral.* **64**, 650–651.

Land L. (1998) Failure to precipitate dolomite at 25 °C from dilute solution despite 1000-Fold oversaturation after 32 years. *Aquat. Geochem.* **4**, 361–368.

Lavoie D., Jackson S. and Girard I. (2014) Magnesium isotopes in high-temperature saddle dolomite cements in the lower Paleozoic of Canada. *Sed. Geol.* **305**, 58–68.

Li W., Beard B. L. and Johnson C. M. (2011) Exchange and fractionation of Mg isotopes between epsomite and saturated $MgSO_4$ solution. *Geochim. Cosmochim. Acta* **75**, 1814–1828.

Li W., Chakraborty S., Beard B. L., Romanek C. S. and Johnson C. M. (2012) Magnesium isotope fractionation during precipitation of inorganic calcite under laboratory conditions. *Earth Planet. Sci. Lett.* **333**, 304–316.

Li W., Beard B. L., Li C. and Johnson C. M. (2014) Magnesium isotope fractionation between brucite [$Mg(OH)_2$] and Mg aqueous species: implications for silicate weathering and biogeochemical processes. *Earth Planet. Sci. Lett.* **394**, 82–93.

Ling M.-X., Sedaghatpour F., Teng F.-Z., Hays P. D., Strauss J. and Sun W. (2011) Homogeneous magnesium isotopic composition of seawater: an excellent geostandard for Mg isotope analysis. *Rapid Commun. Mass Spectrom.* **25**, 2828–2836.

Lowenstein T. K., Timofeeff M. N., Brennan S. T., Hardie L. A. and Demicco R. V. (2001) Oscillations in Phanerozoic seawater chemistry: evidence from fluid inclusions. *Science* **294**, 1086–1088.

Ludwig, K.R., 1999. Using Isoplot/Ex, Version 2.01: a geochronological toolkit for Microsoft Excel. Berkeley Geochronology Center Special Publication 1a, 1–47.

Matsuhisa Y., Goldsmith J. R. and Clayton R. N. (1978) Mechanisms of hydrothermal crystallization of quartz at 250 °C and 15 kbar. *Geochim. Cosmochim. Acta* **42**, 173–182.

Matthews A., Goldsmith J. R. and Clayton R. N. (1983) Oxygen isotope fractionations involving pyroxenes: the calibration of mineral-pair geothermometers. *Geochim. Cosmochim. Acta* **47**, 631–644.

Mavromatis V., Gautier Q., Bosc O. and Schott J. (2013) Kinetics of Mg partition and Mg stable isotope fractionation during its incorporation in calcite. *Geochim. Cosmochim. Acta* **114**, 188–203.

Mavromatis V., Meister P. and Oelkers E. H. (2014) Using stable Mg isotopes to distinguish dolomite formation mechanisms: a case study from the Peru Margin. *Chem. Geol.* **385**, 84–91.

Mottl M. J. and Wheat C. G. (1994) Hydrothermal circulation through mid-ocean ridge flanks: fluxes of heat and magnesium. *Geochim. Cosmochim. Acta* **58**, 2225–2237.

O'Neil J. R. (1986) Theoretical and experimental aspects of isotopic fractionation. *Rev. Mineral.* **16**, 1–40.

Ohtaki H. and Radnai T. (1993) Structure and dynamics of hydrated ions. *Chem. Rev.* **93**, 1157–1204.

Pogge von Strandmann P. A. E., Forshaw J. and Schmidt D. N. (2014) Modern and Cenozoic records of seawater magnesium from foraminiferal Mg isotopes. *Biogeosciences* **11**, 5155–5168.

Rosenberg P. E. and Holland H. D. (1964) Calcite–Dolomite–Magnesite stability relations in solutions at elevated temperatures. *Science* **145**, 700–701.

Rustad J. R., Casey W. H., Yin Q.-Z., Bylaska E. J., Felmy A. R., Bogatko S. A., Jackson V. E. and Dixon D. A. (2010) Isotopic fractionation of Mg^{2+}(aq), Ca^{2+}(aq), and Fe^{2+}(aq) with carbonate minerals. *Geochim. Cosmochim. Acta* **74**, 6301–6323.

Saenger C. and Wang Z. (2014) Magnesium isotope fractionation in biogenic and abiogenic carbonates: implications for paleoenvironmental proxies. *Quat. Sci. Rev.* **90**, 1–21.

Sandberg P. A. (1983) An oscillating trend in Phanerozoic non-skeletal carbonate mineralogy. *Nature* **305**, 19–22.

Schauble E. A. (2004) *Applying Stable Isotope Fractionation Theory to New Systems, Geochemistry of Non-Traditional Stable Isotopes*. Mineralogical Soc America, Washington, pp. 65–111.

Schauble E. A. (2011) First-principles estimates of equilibrium magnesium isotope fractionation in silicate, oxide, carbonate and hexaaquamagnesium(2+) crystals. *Geochim. Cosmochim. Acta* **75**, 844–869.

Shahar A., Young E. D. and Manning C. E. (2008) Equilibrium high-temperature Fe isotope fractionation between fayalite and magnetite: an experimental calibration. *Earth Planet. Sci. Lett.* **268**, 330–338.

Sibley D. F., Nordeng S. H. and Borkowski M. L. (1994) Dolomitization kinetics of hydrothermal bombs and natural settings. *J. Sediment. Res.* **64**, 630–637.

Sofer Z. and Gat J. R. (1972) Activities and concentrations of oxygen-18 in concentrated aqueous salt solutions: analytical and geophysical implications. *Earth Planet. Sci. Lett.* **15**, 232–238.

Spencer R. J. and Hardie L. A. (1990) Control of seawater composition by mixing of river waters and mid-ocean ridge hydrothermal brines. *Spec. Publ. Geochem. Soc.* **19**, 409–419.

Stanley S. M. and Hardie L. A. (1998) Secular oscillations in the carbonate mineralogy of reef-building and sediment-producing organisms driven by tectonically forced shifts in seawater chemistry. *Palaeogeogr. Palaeoclimatol. Palaeoecol.* **144**, 3–19.

Stoffregen R. E., Rye R. O. and Wasserman M. D. (1994) Experimental studies of alunite: II. Rates of alunite-water alkali and isotope exchange. *Geochim. Cosmochim. Acta* **58**, 917–929.

Teng F.-Z., Li W.-Y., Ke S., Marty B., Dauphas N., Huang S., Wu F.-Y. and Pourmand A. (2010) Magnesium isotopic composition of the Earth and chondrites. *Geochim. Cosmochim. Acta* **74**, 4150–4166.

Tipper E. T., Galy A., Gaillardet J., Bickle M. J., Elderfield H. and Carder E. A. (2006) The magnesium isotope budget of the modern ocean: constraints from riverine magnesium isotope ratios. *Earth Planet. Sci. Lett.* **250**, 241–253.

Urey H. C. (1947) The thermodynamic properties of isotopic substances. *J. Chem. Soc.*, 562–581.

Vail P. R., Mitchum R. M. and Thompson S. (1977) Seismic stratigraphy and global changes of sea-level, Part 4: global cycles of relative changes of sea level. *Am. Assoc. Pet. Geol. Mem.* **26**, 83–97.

Vasconcelos C., McKenzie J. A., Bernasconi S., Grujic D. and Tiens A. J. (1995) Microbial mediation as a possible mechanism for natural dolomite formation at low temperatures. *Nature* **377**, 220–222.

Warren J. (2000) Dolomite: occurrence, evolution and economically important associations. *Earth Sci. Rev.* **52**, 1–81.

Wilkinson B. H. and Algeo T. J. (1989) Sedimentary carbonate record of calcium-magnesium cycling. *Am. J. Sci.* **289**, 1158–1194.

Young E. D. and Galy A. (2004) The isotope geochemistry and cosmochemistry of magnesium. *Rev. Mineral. Geochem.* **55**, 197–230.

Young E. D., Manning C. E., Schauble E. A., Shahar A., Macris C. A., Lazar C. and Jordan M. (2015) High-temperature equilibrium isotope fractionation of non-traditional stable isotopes: experiments, theory, and applications. *Chem. Geol.* **395**, 176–195.

Zenger, D.H., Dunham, J.B., Ethington, R.L., 1980. Concepts and models of dolomitization, Spec. Publ. -SEPM 28. Society of Economic Paleontologists and Mineralogists, Tulsa, OK, p. 320.

Zhang F., Xu H., Konishi H. and Roden E. E. (2010) A relationship between d104 value and composition in the calcite-disordered dolomite solid-solution series. *Am. Mineral.* **95**, 1650–1656.

Zhang F., Xu H., Konishi H., Kemp J. M., Roden E. E. and Shen Z. (2012a) Dissolved sulfide-catalyzed precipitation of disordered dolomite: implications for the formation mechanism of sedimentary dolomite. *Geochim. Cosmochim. Acta* **97**, 148–165.

Zhang F., Xu H., Konishi H., Shelobolina E. S. and Roden E. E. (2012b) Polysaccharide-catalyzed nucleation and growth of disordered dolomite: a potential precursor of sedimentary dolomite. *Am. Mineral.* **97**, 556–567.

Associate editor: Jeffrey C. Alt